AN ABSTRACT OF THE THESIS OF

MARSHALL DELPH EARLE (Name) for the DOCTOR OF PHILOSOPHY (Degree)

in OCEANOGRAPHY (Major) presented on 11 March 1971 (Date)

Title: A THREE COMPONENT DRAG PROBE FOR THE MEASUREMENT OF OCEAN WAVE ORBITAL VELOCITIES AND TURBULENT WATER VELOCITY FLUCTUATIONS

Redacted for privacy

Abstract approved: Dr. S. Pond

A three component drag probe has been built, calibrated, and used to measure velocities beneath deep water ocean waves and turbulence in a tidal channel. Simple variable inductance devices which may be submerged in water were used as displacement transducers and the associated electronics provided voltage outputs which were proportional to the three components of force that were exerted on a small 5 cm diameter sphere. The force components were due to both the water drag force and the water inertial force in an accelerating flow field. Techniques are described for interpreting measurements made with the drag probe and for obtaining the three velocity components from the measured force components. From the drag probe calibration and its use in the field, it is concluded that the drag probe is a suitable instrument for the measurement of wave velocities

and turbulence. Modifications are suggested to improve the performance of the drag probe.

For the wave velocity measurements, the experimental results indicate that linear wave theory is adequate to describe the relations between the wave pressure and the wave velocity components. At frequencies higher than the predominant wave frequency the velocity spectra are rougly proportional to f^{-3} where f is the frequency in Hz. The wave velocity components were used to obtain an estimate of the directional energy spectrum.

From the measurements in a tidal channel, it appears that the instrument is suitable to measure turbulent fluctuations with scale sizes larger than about 20 cm. If the turbulence were isotropic the velocity spectra would be proportional to $f^{-5/3}$. Due to the influence of boundaries, the flow was not isotropic but the results appear to be consistent with other observations that turbulent velocity spectra usually show a f^{-1} to f^{-2} behavior and are quite different from wave velocity spectra.

A Three Component Drag Probe for the Measurement of Ocean Wave Orbital Velocities and Turbulent Water Velocity Fluctuations

by

Marshall Delph Earle

A THESIS

submitted to

Oregon State University

in partial fulfillment of
the requirements for the
degree of

Doctor of Philosophy

June 1971

APPROVED:

Redacted for privacy

Associate Professor of Oceanography

in charge of major

Redacted for privacy

Chairman of Department of Oceanography

Redacted for privacy

Dean of Graduate School

Date thesis is presented 11 March 71

Typed by Clover Redfern for Marshall Delph Earle

ACKNOWLEDGMENT

I am deeply indebted to Dr. George F. Beardsley, Jr., under whom I carried out this research. I especially thank Dr. G. Stephen Pond whose help was indispensable during the final phases of this research after Dr. Beardsley's death. I wish to thank Mr. Jack Groelle who built the drag probe. I am grateful to Dr. M. N. L. Narasimhan, Dr. J. H. Nath, and Dr. F. L. Ramsey for their helpful discussions and suggestions.

During my graduate studies, I was supported by a National Defense Education Act Fellowship. This research was funded by the National Science Foundation under Grant GA 998.

TABLE OF CONTENTS

Chapter		Page
I.	INTRODUCTION	1
	Importance of the Measurements	1
	Types of Sensors	3
	Instrument Requirements	6
II.	THE THREE COMPONENT DRAG PROBE	8
	Theory of Operation	8
	Description of the Instrument	10
	Displacement Transducers and Restoring Force	11
	Drag Probe Electronics	13
	Drag Probe Assembly	16
	Frequency Response Characteristics	18
	Calibration of the Instrument	20
	Response to Static Forces	20
	Response to Water Drag and Inertial Forces	22
III.	TECHNIQUES TO OBTAIN VELOCITY COMPONENTS FROM DRAG PROBE MEASUREMENTS	31
	Interpretation of Drag Probe Measurements	31
	Use of the Drag Probe Beneath Surface Gravity Waves	31
	Use of the Drag Probe to Measure Turbulence	33
	A Numerical Technique to Obtain the Velocity Components	36
IV.	THEORY APPLICABLE TO THE MEASUREMENTS	43
	Linear Wave Theory and Wave Statistics	43
	Turbulence Theory	48
V.	VELOCITY MEASUREMENTS BENEATH DEEP WATER OCEAN WAVES	51
	Description of Experiment	51
	Data Collection and Processing	51
	Results	56
VI.	TURBULENCE MEASUREMENTS IN A TIDAL CHANNEL	69
	Description of Experiment and Analysis	69
	Results	69

Chapter		Page
VII.	DISCUSSION AND CONCLUSIONS	81
	Experimental Results	81
	Suggested Drag Probe Modifications	82
	BIBLIOGRAPHY	85

LIST OF TABLES

Table		Page
1.	Typical test of numerical procedure.	42
2.	Spectral results for wave data.	55
3.	Spectral results for tidal channel data, run 1.	72
4.	Spectral results for tidal channel data, run 2.	73

LIST OF FIGURES

Figure		Page
1.	Three component drag probe.	12
2.	Drag probe electronics.	14
3.	Drag probe response to static forces.	21
4.	Typical calibration record.	25
5.	Drag probe response to water acceleration.	26
6.	Drag probe response to water velocity.	28
7.	TOTEM experimental arrangement.	52
8.	Vertical velocity and pressure cumulative probability distributions.	59
9.	Velocity and pressure spectra.	61
10.	Pressure and vertical velocity spectra.	64
11.	Directional energy spectra.	67
12.	Tidal channel experimental arrangement.	70
13.	Velocity spectra, run 1.	75
14.	Velocity spectra, run 2.	76

A THREE COMPONENT DRAG PROBE FOR THE MEASUREMENT OF OCEAN WAVE ORBITAL VELOCITIES AND TURBULENT WATER VELOCITY FLUCTUATIONS

I. INTRODUCTION

Even in 1971, there have been relatively few direct measurements of water velocity fluctuations at frequencies within and above the surface gravity wave frequency band. The main problem has been the development of a sensor with a sufficiently small size and a sufficiently high frequency response to measure these fluctuations and also sturdy enough to withstand current and wave motion and rough handling in the field.

Importance of the Measurements

Direct measurements of the velocities associated with surface gravity waves are needed to study the wave forces which are exerted on structures and the relations between the velocities and other wave parameters such as the wave height, wave pressure, and wave slopes. For instance, it is difficult to determine the wave forces exerted on piles from measurements of the wave height and the wave pressure. As Wiegel (1964, p. 256) shows, there is considerable scatter of the empirically determined drag and inertia coefficients which relate the wave forces to the wave velocities and accelerations. The wave

velocities and accelerations are usually computed from measurements of the wave height and pressure and, if the wave velocities can be more accurately computed, a major source of error can be eliminated from the force calculations that are presently used. With a better description of the velocity field, it may be possible to reduce the scatter of the computed drag and inertia coefficients. The relations between the wave velocities and other wave parameters have not been adequately studied and compared to the various wave theories. In addition, where such relations have been or can be established, measurements of the wave velocities can be used to infer desired information about the wave surface.

Turbulence plays an important part in numerous oceanic phenomena. In tidal channels, turbulence determines the momentum fluxes and influences the movement of sediment and the suspension of sediment within the water column. In the upper ocean, turbulence is involved in the exchange of properties with the atmosphere, the mixing of properties, the structure of the thermocline and the dissipation of surface and internal wave energy. Direct measurements of upper ocean turbulence can yield information about the exchange of momentum, heat, and water vapor to and from the atmosphere above and the transfer of momentum, heat, and salt to and from the deeper ocean below. Studies of turbulence are vital to an understanding of the dynamics of the upper layers of the ocean and, hence, of the whole

ocean.

Types of Sensors

Numerous water velocity sensors have been developed for use at sea or in tidal channels. Hot wire, hot film, and hot thermistors all rely on resistance changes of the sensor due to the cooling of the sensor by the moving water. Hot wire and hot film devices have been used to measure turbulence by Patterson (1958), Grant et al. (1962), and Stewart and Grant (1962). These devices can have a very wide frequency response but can become coated with plankton during operation and are basically one component devices. It is difficult to use an array of several hot wires or hot films to obtain three velocity components without disturbing the flow. Hot thermistors have been used by Eagleson and Van der Watering (1964) to measure wave orbital velocities in a wave tank and by Lukasik and Grosch (1963) to measure wave orbital velocities near the bottom in shallow water. Because hot thermistors respond to the magnitude of the velocity, there is no way to obtain the velocity components. Shonting (1967) used ducted rotor sensors to measure wave velocities in shallow water. A ducted rotor sensor consists of a propeller in a cylindrical housing. Speeds are obtained by counting the number of rotor revolutions and the flow direction is obtained from the direction in which the propeller is rotating. Although ducted current meters are simple and reliable,

they are difficult to manufacture with sizes of a few cm, their response times are not always low enough for fluctuating flows in which the propeller must often change direction, and they have a complicated directional response. In order to measure three dimensional velocity fluctuations, one must use three ducted current meters and the flow may be distrubed. Electromagnetic flow meters which generate a magnetic field and measure induced voltages caused by the movement of the water have been used to measure turbulence in tidal channels by Bowden and Fairbairn (1956) and Bowden (1962) and to measure wave orbital velocities in shallow water by Nagata (1964), Bowden and White (1966), and Simpson (1969). The electromagnetic flow meters used in the measurements were roughly spherical in shape with diameters of approximately 10 cm. Because two sensors are required to measure three velocity components, it is hard to measure small scale fluctuations without disturbing the flow. Miller and Zeigler (1964) have used an ultrasonic sensor to measure wave velocities in the surf zone. An ultrasonic sensor detects the Doppler shift of sound waves which is caused by the motion of the water. Ultrasonic sensors are fairly expensive and, if built to measure three velocity components, are difficult to make sufficiently rugged without disturbing the flow.

Drag probes which measure the force exerted on the sensor have been used to determine wave velocities in shallow water by

Inman and Nasu (1956) and to measure velocities in a wave tank by Beardsley et al. (1963). Both of these sensors were two direction devices which measured the deflection of a rod. Suzuki (1969) and Grace and Casciano (1969) have measured the horizontal wave forces on spheres placed near the bottom in shallow water. Because the sphere used by Suzuki was about 50 cm in diameter and the sphere used by Grace and Casciano was 20 cm in diameter, these instruments would not be suitable to measure small scale fluctuations.

In the atmosphere, spherical three component drag probes, also called thrust anemometers, have been developed for turbulence measurements (Doe, 1963; Smith, 1966, 1967; Kirwan et al., 1966; Adelfang, 1969; McNally, 1970). These instruments are all less than 10 cm in diameter, have been calibrated in wind tunnels, and measure the three components of wind force acting on a sphere. From these force components, the velocity components can be computed. Smith (1966, 1967) has made extensive turbulence measurements in the boundary layer above the sea with a thrust anemometer and has demonstrated that his instrument gives results in close agreement with those of other sensors such as cup anemometers and hot wires. Because of their electrical and mechanical construction, the thrust anemometers as they have been built cannot be used for measurements of water velocities.

Instrument Requirements

The primary requirements for an instrument which is to measure wave orbital velocities and turbulence are: 1. that the sensor have a high frequency response so that no amplification or attenuation of the true signal occurs, 2. that the sensor be small enough to obtain good spacial resolution, and 3. that the instrument be sturdy and compact so that it can be used at sea. The frequencies of surface gravity waves are generally less than 1 Hz (cycles per second) and the wavelengths are usually greater than 1 m. The sensor should have a frequency response several times greater than 1 Hz and a size several times smaller than 1 m to measure wave particle velocities. For measurements of turbulence, the requirements are much more stringent. The measurements of Stewart and Grant (1962) indicate that a frequency response to 20 Hz is probably sufficient to obtain the inertial subrange of turbulence. The sensor should also have a size about five times smaller than the scale sizes of the turbulence which the sensor is to measure. Because of the small size requirement, some of the sensors which have been discussed are not suitable for turbulence measurements. As an example, ducted current meters and electromagnetic flow meters are often suitable for measurements of wave particle velocities but not for measurements of all turbulence scales.

The thrust anemometers which have been used in the atmosphere have the advantages of having high frequency responses, being sturdy and of fairly small size, and yielding the three components of force from which the three components of velocity can be obtained. Such sensors used underwater can be useful for both wave and many turbulence measurements. This thesis describes such an instrument and measurements made beneath deep water ocean waves and of tidal channel turbulence.

II. THE THREE COMPONENT DRAG PROBE

Theory of Operation

As shown in the sections describing the drag probe and its electronics, the drag probe is an instrument which provides voltage outputs E_i which depend on the forces F_i exerted on an almost spherical object. If the probe is rigidly suspended within a flow field, the forces F_i are assumed to be

$$F_i = \frac{1}{2} \rho A_i C_D u_i |\vec{u}| + \rho C_M V \frac{du_i}{dt} \qquad i = 1, 2, 3 \qquad (1)$$

where ρ is the water density, A_i is the projected cross-sectional area of the object in the ith direction, u_i is the ith component of water velocity $\vec{u}$, C_D is the drag coefficient which is a function of $|\vec{u}|$, the magnitude of $\vec{u}$, C_M is the inertia coefficient, V is the volume of the object, and du_i/dt is the ith component of the total water acceleration. The first term in Equation 1 is the drag force and the second term is the inertial force. O'Brien and Morison (1952) discuss Equation 1 and have verified the equation for spheres beneath surface waves in a wave tank. O'Brien and Morison found the drag coefficient C_D to be a function of $|\vec{u}|$ and the inertia coefficient C_M to be independent of $|\vec{u}|$. As later shown, the calibration of the drag probe yielded the same results: C_D was a function

of $|\vec{u}|$ and C_M was independent of $|\vec{u}|$. The three component equations described by Equation 1 are coupled together by the magnitude of the velocity. To see that the velocity magnitude is necessary, consider the drag force exerted on a sphere of cross-sectional area A. The vector form of the drag force term in Equation 1 is

$$\vec{F}_{drag} = \frac{1}{2}\rho A C_D |\vec{u}|^2 \frac{\vec{u}}{|\vec{u}|} \tag{2}$$

Equation 2 shows that the drag force depends on the magnitude of the velocity and is in the direction of the flow velocity $\vec{u}$. The magnitude of the drag force is independent of the direction of the velocity $\vec{u}$.

The voltage outputs E_i of the drag probe are related to the forces F_i by the following equation

$$E_i = h_i F_i + e_i \qquad i = 1, 2, 3 \tag{3}$$

where each h_i is a constant and each e_i is a constant voltage offset due to the drag probe electronics. The following equation thus relates the voltage outputs E_i to the water velocity and acceleration

$$E_i - e_i = B_i C_D u_i |\vec{u}| + H_i \frac{du_i}{dt} \qquad i = 1, 2, 3 \tag{4}$$

in which

$$B_i = \frac{1}{2}\rho A_i h_i$$

and

$$H_i = \rho C_M V h_i$$

There are two contributions to the inertial term in Equation 4 (Lamb, 1945, p. 123) and the coefficient H_i can be written as

$$H_i = \rho C_M V h_i = h_i(M_0+M_V) \qquad i = 1, 2, 3 \tag{5}$$

where M_0 is the mass of the displaced water ρV and M_V is called the virtual mass. The first term in $H_i du_i/dt$, $h_i M_0 du_i/dt$, is due to the pressure gradient force exerted on the object due to the water particle acceleration and the second term, $h_i M_V du_i/dt$, is due to the pressure distribution caused by the disturbance to the flow acceleration by the object.

Description of the Instrument

The simplest method to measure the force exerted on an object is to provide a restoring force and to measure the displacement of the object. The thrust anemometers which have been used in the atmosphere use springs to provide the restoring forces and strain gauges or differential transformers as displacement transducers. For underwater use, it is very difficult to insulate such displacement transducers from the water. It was thus necessary to design a displacement transducer which could be exposed to the water and which would

be very small. In addition the associated circuit must be simple and easily packaged in a small electronics case. Because the drag probe may be installed at sea by divers it must be both durable and easily repairable.

Displacement Transducers and Restoring Force

Figure 1 shows a drawing of a complete drag probe. The probe head consists of an inner sphere which is rigidly attached to its support and a outer roughly spherical shell which surrounds the inner sphere and is connected to it by compressed sponge rubber supports. As is shown by a calibration later described, this rubber provides a restoring force so that the displacement of the outer sphere with respect to the inner sphere is proportional to the force exerted on the outer sphere. By measuring the displacements in three mutually perpendicular directions, one can thus obtain three components of force acting on the outer sphere.

Variable inductance devices are used as displacement transducers and the associated electronics provide voltage outputs which are proportional to the relative displacements of the two spheres in three directions. For each component, the displacement transducer consists of a ferrite disk which is attached to the outer sphere and a ferrite core inductor which is molded within the inner sphere and is part of the probe electronics. The axis of each inductor is

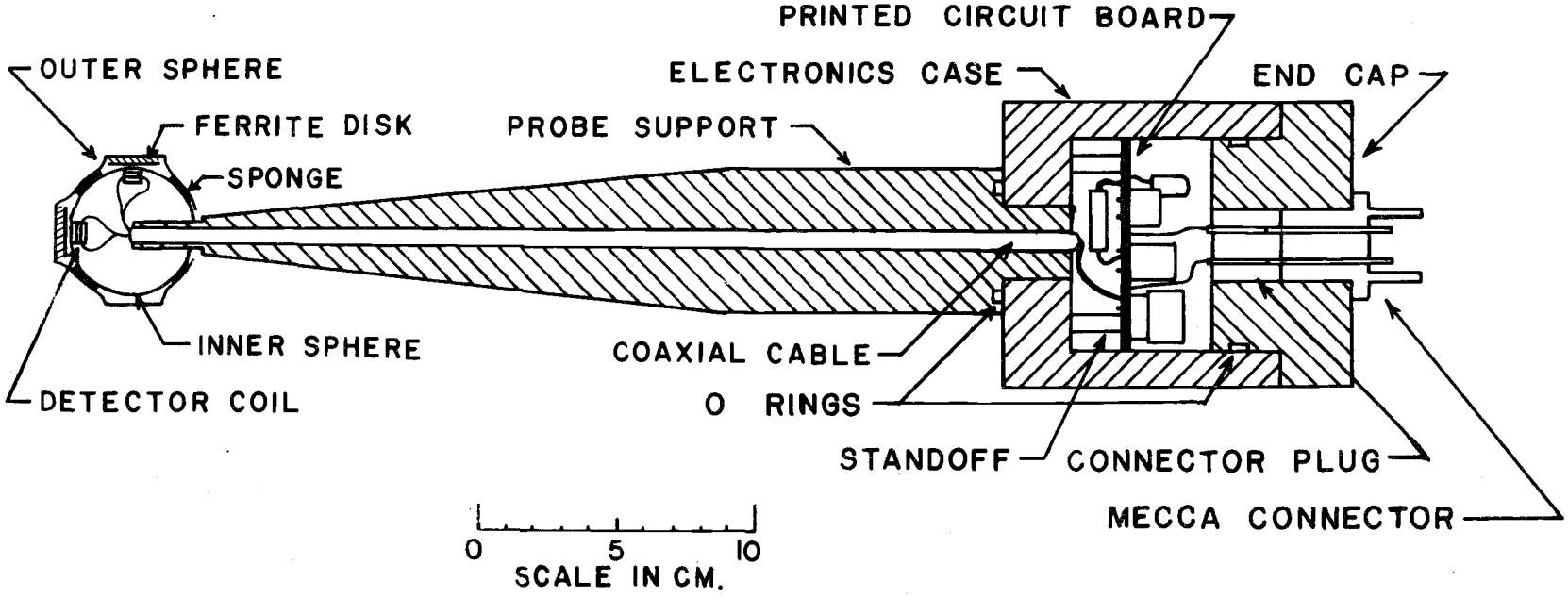

Figure 1. Three component drag probe.

perpendicular to the plane of the disk which is centered above the inductor. The inductance depends upon the distance between the disk and the inductor. The ferrite disks are 2.54 cm in diameter and 0.13 cm thick.

Figure 1 shows two of the disks attached to the outer sphere and the arrangement of the inductors within the inner sphere. A third disk and inductor lie along an axis perpendicular to the page. A 1.5 cm diameter hole in one side of the outer sphere allows the support to reach the inner sphere and also allows water to fill the space between the spheres.

Drag Probe Electronics

The drag probe electronics are shown in Figure 2 and are contained within the probe assembly that is shown in Figure 1. A 700 kHz Colpitts oscillator provides a sinusoidal 24 V peak-to-peak signal at the collector of the oscillator silicon transitor (T1S97). Capacitors C_3 and C_4 and inductor L_1 are the frequency determining components of the oscillator. Voltage divider R_4, coupling capacitor C_6, and FET bias setting resistors R_5 and R_6 convert the 24 V signal to a 2.5 V peak-to-peak 700 kHz signal superimposed upon a -8 V dc bias level. The 2.5 V signal drives three FET common source unity gain amplifiers (2N3819), which have high input impedances to provide isolation between the probe channels and low output

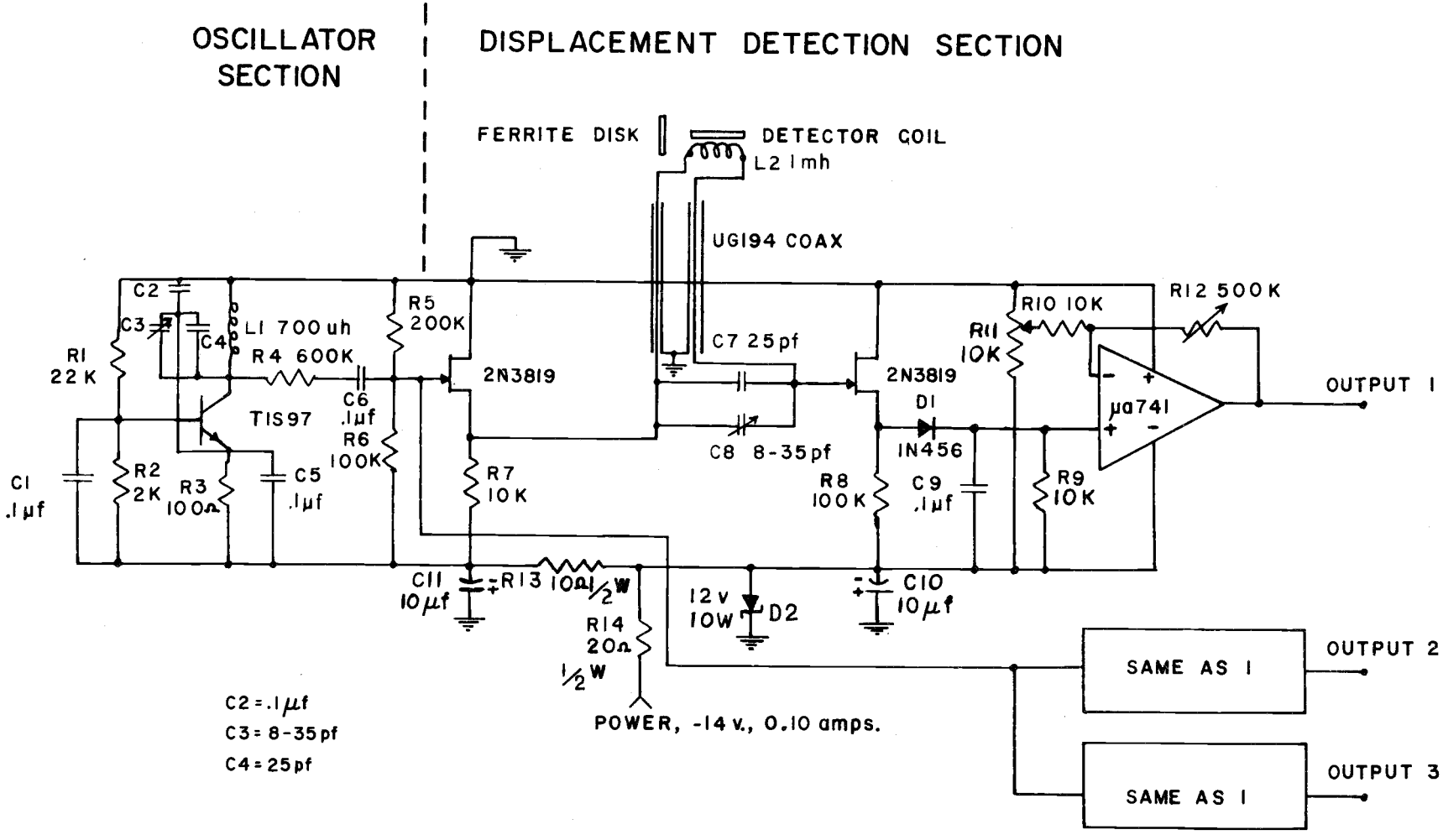

Figure 2. Drag probe electronics.

impedances to drive the detector circuits.

Each detector circuit is a tuned resonant tank circuit. For the typical channel shown in Figure 2, the detector circuit consists of inductor L_2 and capacitors C_7 and C_8. Inductor L_2 is made by winding No. 36 enameled wire on a plastic bobbin which is then fitted within a half-section of an E pot ferrite form. Three such inductors are fitted within the inner sphere so that they face in mutually perpendicular directions with the bottoms of the E pot forms toward the center of the sphere. The half-section of ferrite material is necessary to prevent magnetic coupling between the three channels. If a ferrite disk is centered over inductor L_2 and if this disk is moved inward or outward, the impedance of the resonant circuit changes and thus the peak-to-peak output voltage at the gate of the second FET common source unity gain amplifier also changes. After passing through this FET common source unity gain amplifier (2N3819) which provides a high input impedance for the output of the detector circuit, the voltage is rectified by diode D_1. Filtering is provided by capacitor C_9. Capacitor C_9 and resistor R_9 determine the rectifier time constant (1 msec) and may be changed if a different time constant is desired.

The final operational amplifier stage provides the desired dc offset and gain and drives the cable connecting the probe to the recording apparatus. The operational amplifiers are Fairchild μA741

internally compensated integrated circuit types. Resistor R_{11} determines the dc offset and resistor R_{12} determines the gain.

The supply voltage should be between -12 V and -14 V with respect to ground. This voltage is regulated to -12 V by Zener diode D_2. The current drain is 0.10 A. The change in output voltage of the circuit in the 4°-22°C region where the probe is to be used is 0.1%/C°.

Drag Probe Assembly

The inner sphere that is shown in Figure 1 is molded directly to the probe support. The three inductor coils are attached to the interior of a spherical mold and the coil leads are soldered to coaxial cables which pass through the probe support. The support is clamped into the mold and the mold is filled with a clear polyester resin. When the resin is dry the mold is removed.

The probe support and the pressure case for the electronics are machined from solid cylindrical sections of PVC material. The end cap of the electronics case is easily removed so that adjustments can be made on the electrical circuits. 0-rings insure water tight seals between all removable parts. Electrical connections are made through a six pin Mecca underwater connector on the end cap.

Each half of the outer sphere shown in Figure 1 is made from a 7.6 cm square section of clear 0.07 cm thick Plexiglas. The desired

half-spherical shape is cut into an aluminum block and the Plexiglas sheet is attached to the top of the block. The Plexiglas is heated with a heat gun and, as the Plexiglas buckles, the interior of the mold is evacuated until the Plexiglas is pulled tightly against the interior surface of the mold. To form the protrusions which hold the ferrite disks, a wooden dowel is used to press the Plexiglas into indentations on the interior surface of the mold. After two sections have been made with the mold, the three ferrite disks are epoxied to one of the half-spherical sections. A special jig is used to insure that the three disks are mutually perpendicular.

The restoring force between the spheres is provided by twelve 1.9 x 1.9 cm squares of approximately 1.2 cm thick self-adhering sponge rubber weather stripping. The covering is peeled from the squares and the squares are attached in a symmetrical manner directly to the inner sphere. After coating the outer faces of the squares with plastic rubber, the outer sphere sections are assembled over the inner sphere so that each ferrite disk is directly over and parallel to the corresponding detector coil within the inner sphere. During this process, the sponge rubber surrounding the inner sphere is compressed to a thickness of approximately 0.6 cm. The outer sphere sections are finally glued together with a plastic glue designed for Plexiglas. Although the outer sphere has only three ferrite disks attached to it, it is approximately symmetrical with corresponding

protrusions on each side. The slight asymmetry is due to manufacturing difficulties. The mass of the outer sphere with its three ferrite disks is 13.2 g. Neglecting its disk holding protrusions, its diameter is 5.0 cm.

Frequency Response Characteristics

To determine the frequency response characteristics, the drag probe was submerged in water and a screwdriver was used to sharply rap each axis. The outputs were recorded on an oscillograph at a high chart speed and damped resonant oscillations were found on the chart records. The damped resonant frequencies for all axes were about 18 Hz. By considering each axis as a simple one degree of freedom damped harmonic oscillator and measuring the relative decay of oscillation (see, for example, Thomson, 1965, p. 43), the relative damping for all three axes was found to be 0.5. The relative damping ζ is related to the logarithmic decrement δ by

$$\delta = \frac{2\pi\zeta}{[1-\zeta^2]^{1/2}} \tag{6}$$

and $\delta = \ln (x_1/x_2)$ where x_1 and x_2 are the first and second peak values observed. From the observed value of δ, obtained by averaging x_1/x_2 values from several trials, ζ is obtained from a graph of Equation 6 given in Thomson (1965). When $\zeta = 1$, the

oscillator is critically damped and, for $\zeta < 1$, the oscillator is underdamped. The relation between the damped resonant frequency f_d obtained by striking the probe and the natural undamped resonant frequency f_n is

$$f_d = [1-\zeta^2]^{1/2} f_n \tag{7}$$

The natural resonant frequencies for all axes were about 21 Hz.

If a sinusoidal force $F_0 \sin(2\pi ft)$ where F_0 is constant is applied to a simple one degree of freedom damped harmonic oscillator, the phase ϵ between the applied force and the displacement of the oscillator after transients have disappeared is given by

$$\epsilon = \tan^{-1} \left[\frac{2\zeta(f/f_n)}{1-(f/f_n)^2} \right] \tag{8}$$

For a natural frequency of 21 Hz and a relative damping of 0.5 the phase shift is 8° for $f = 3$ Hz and is less than 2° when f is less than 1 Hz. For measurements of forces due to gravity waves, phase shifts are thus negligible. For measurements of high frequency turbulence, phase shifts may not be negligible. However each axis of the drag probe has almost the same relative damping and natural resonant frequency and thus the relative phases between the three axes are preserved.

For a simple one degree of freedom damped harmonic oscillator with an applied sinusoidal force $F_0 \sin(2\pi f)$ where F_0 is constant, the ratio of the amplitude of the displacement x_s after transients have disappeared to the ideal displacement amplitude x_0 is

$$\frac{x_s}{x_0} = [(1-(f/f_n)^2)^2 + (2\zeta(f/f_n))^2]^{-1/2} \qquad (9)$$

For a natural frequency of 21 Hz and a relative damping of 0.5, Equation 9 has values from unity to 1.03 for frequencies below 5 Hz, rises to 1.16 at 14 Hz and then falls toward zero. The 3 db point is defined by $x_s/x_0 = 0.707$ and the 3 db point for all axes was about 28 Hz.

Calibration of the Instrument

Response to Static Forces

Figure 3 shows the responses to static forces which were obtained by using a spring scale to displace the outer sphere. The offset voltages e_i due to the drag probe electronics have been removed. Axes 1 and 2 form a plane which is perpendicular to the probe support and which passes through the center of the sphere. Axis 3 passes through the center of the sphere in the direction of the probe support. Crosstalk, erroneous voltage outputs from one axis due to the force exerted on another axis, was measured during the static force tests.

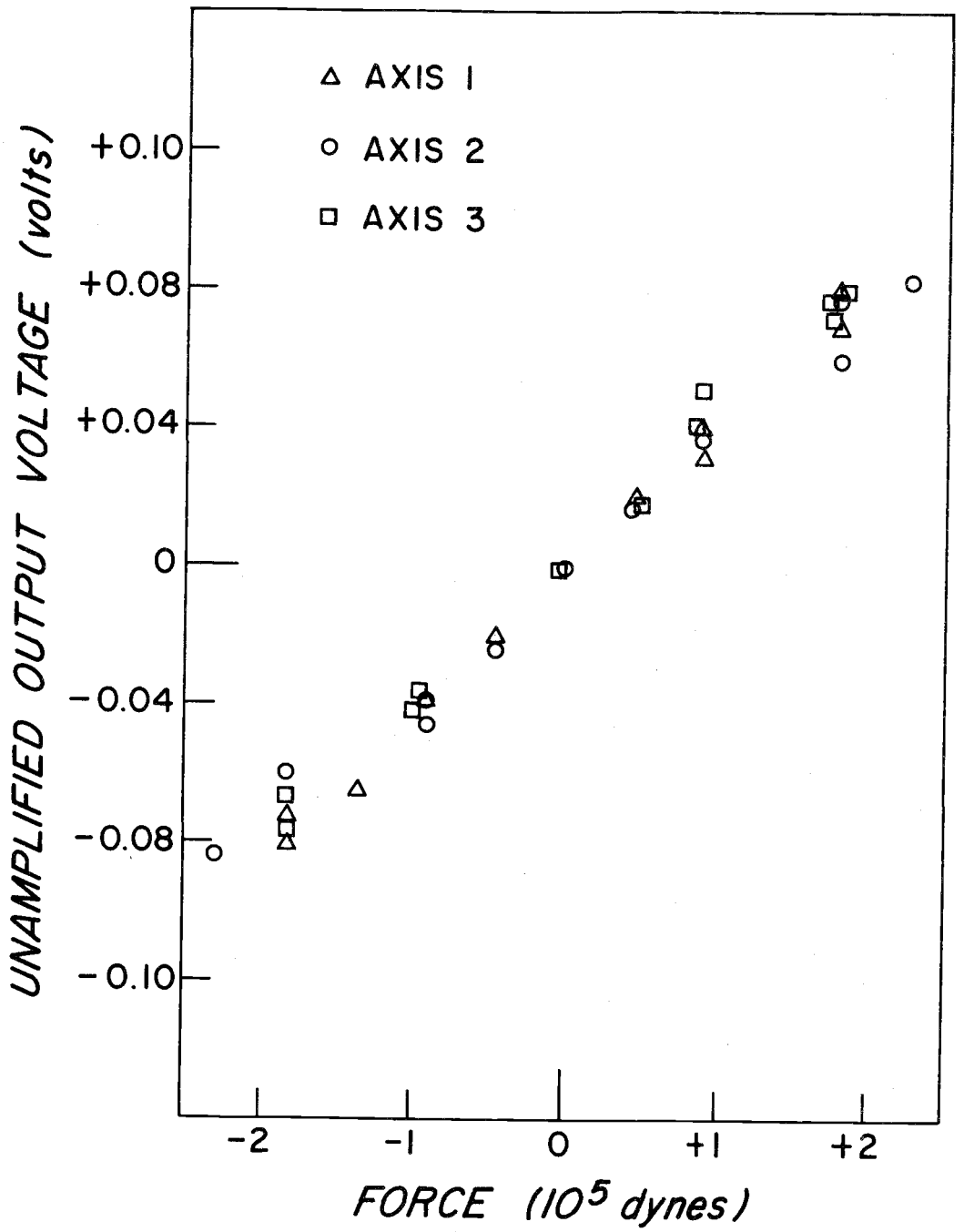

Figure 3. Drag probe response to static forces.

For forces up to 2×10^5 dynes upon a given axis, the voltage outputs of the other axes deviated from their equilibrium positions by less than 3% of their 2×10^5 dyne deviations. For all axes, a force of 2×10^5 dynes is approximately equivalent to the drag force produced by a 200 cm-sec^{-1} water velocity. The crosstalk is likely due to the planes of the disks not being exactly parallel to the axes of their corresponding inductors. The crosstalk could probably be reduced by more careful manufacture of the sensor head.

Hysteresis, the failure of the outer sphere to return to its equilibrium position, was observed during the static force tests. For axes 1 and 3, the hysteresis for forces up to 2×10^5 dynes was less than 3% of the total displacement. For axis 2, the hysteresis for forces up to 10^5 dynes was less than 3% of the total displacement but, for forces up to 2×10^5 dynes increased to 10% of the total displacement. In field use, axis 2 was therefore aligned vertically so that it would not be exposed to any large mean forces. The hysteresis is caused by the compressed sponge rubber supports and is a major shortcoming of the present sensor.

Response to Water Drag and Inertial Forces

The drag probe response to water drag and inertial forces was determined by attaching the probe to a pendulum (length = 3.5 m) and oscillating the probe at various frequencies and amplitudes in a

circular water filled tank (diameter = 1.8 m, depth = 0.9 m). The top of the pendulum was connected to an inverted gyroscope mounting attached to the ceiling and, as the pendulum was swung, wiper pots in the gyroscope mounting had resistances proportional to the angular displacements of the pendulum in two directions. A simple voltage divider circuit was used to provide voltages proportional to the angular displacements of the pendulum. The angular displacements of the pendulum and the voltage outputs of the drag probe were recorded. From the pendulum length and records of the angular displacements, the velocity and acceleration of the water with respect to a coordinate system aligned with the axes of the probe were obtained. The drag probe was calibrated by determining the relations between the drag probe voltage outputs and the water velocity and acceleration with respect to the probe.

The pendulum was generally swung by hand in either a plane or in an elliptical orbit. By observing the angular displacements on an oscilloscope or chart recorder, an approximately sinusoidal motion could be obtained. To minimize movement of the water with respect to the tank, the pendulum was frequently stopped. In calibrating axes 1 and 2 which are perpendicular to the probe support, only the force sensing sphere of the probe was submerged. The depth of the sphere below the water surface was about 30 cm. To calibrate axis 3 which is along the axis of the probe support, it was necessary to submerge

the entire probe assembly. Calibration data were obtained for pendulum oscillations with frequencies from 1.3 Hz to 0.1 Hz, and peak-to-peak amplitudes from 10 cm to 175 cm. Because the pendulum oscillation frequencies were far below the natural resonant frequencies of the drag probe, the measured forces were due to the water drag and inertial forces. Figure 4 shows a typical calibration record.

In order to investigate the inertial force term in Equation 4, time points from the calibration records were selected when the velocity in the direction of a given axis was zero. Such time points occurred when the pendulum was at a maximum displacement in the direction of the given axis. As is shown in Equation 5, there are two contributions to the inertial term in Equation 4. Only the $h_i M_V$ contribution is obtained if the probe is oscillated in a tank (Lamb, 1945, p. 644). Figure 5 is a plot of the voltage outputs vs the corresponding acceleration at time points when the velocity for the given axis was zero. The offset voltages e_i due to the drag probe electronics have been removed. The $h_i M_V$ contribution to each H_i was found from the least squares slopes of the data which is plotted in Figure 5. The $h_i M_0$ contribution to each H_i was calculated from the outer sphere dimensions.

The drag force term in Equation 4 was investigated by selecting time points from the calibration records when the acceleration in the direction of a given axis was zero. Such time points occurred when

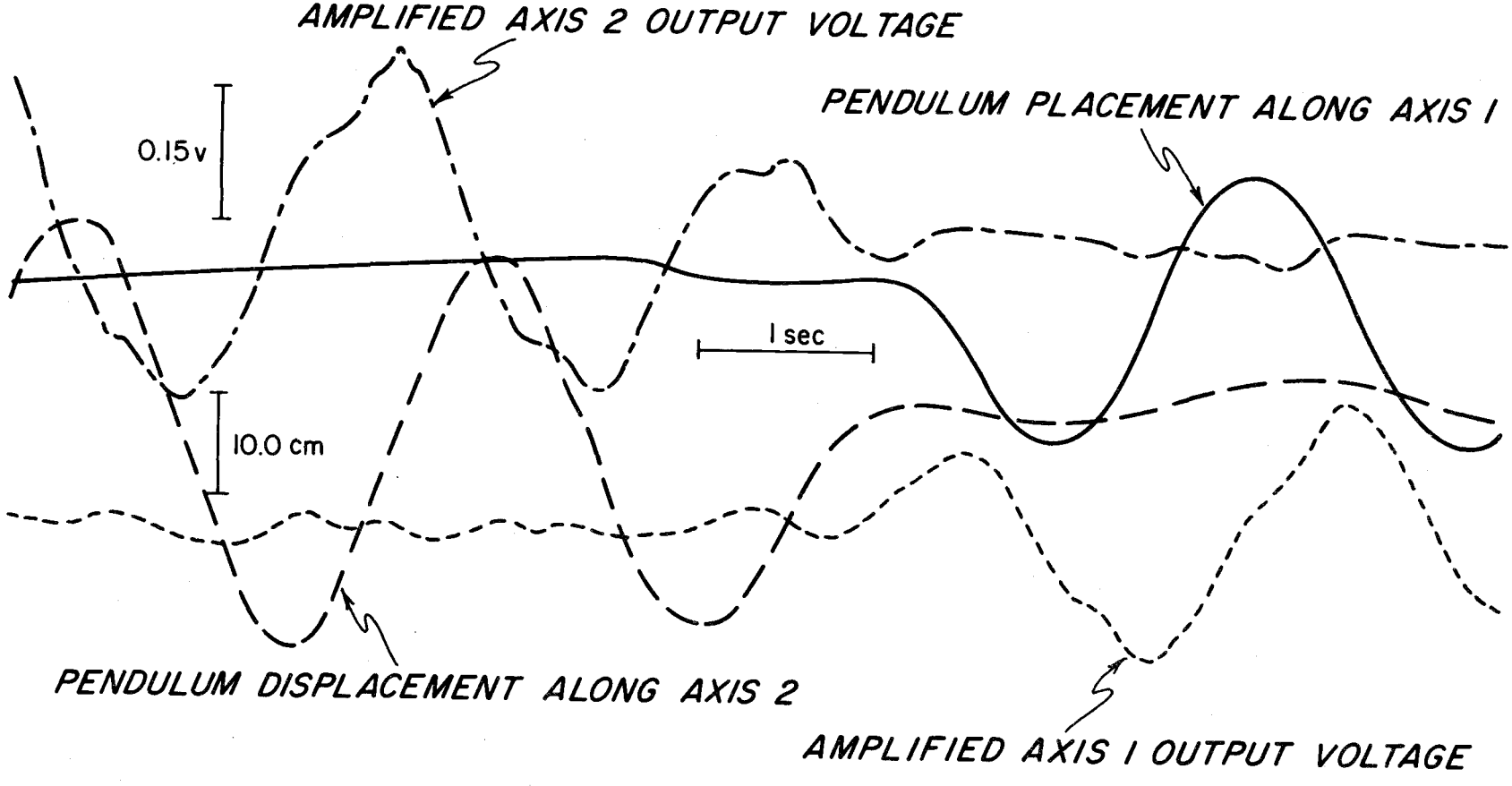

Figure 4. Typical calibration record.

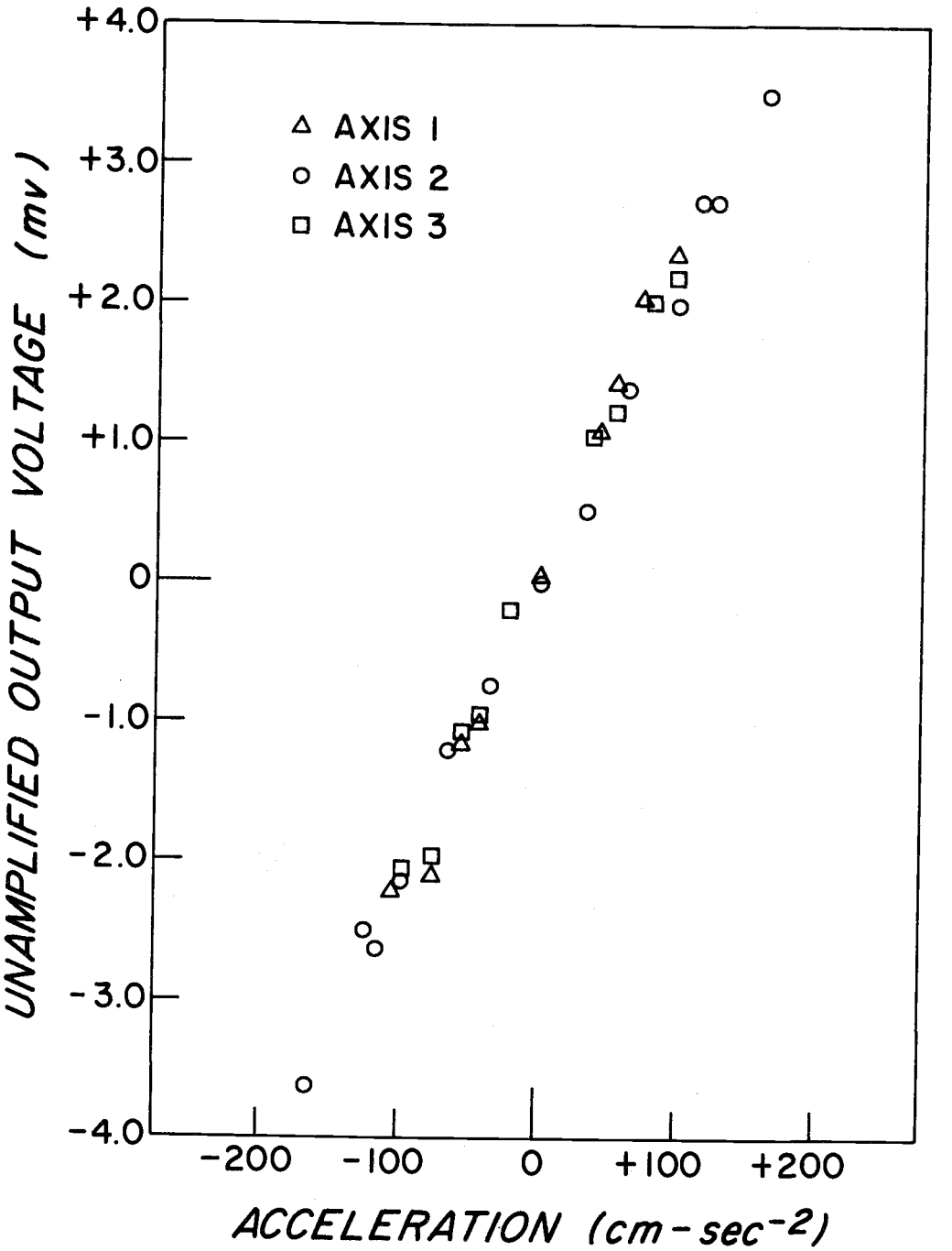

Figure 5. Drag probe response to water acceleration.

the pendulum was moving through the vertical position. Figure 6 is a log-log plot of the magnitude of the voltage outputs vs the magnitude of the corresponding velocity when the velocity was only in the direction of the given axis. The offset voltages e_i have been removed. By fitting least squares lines to the data shown in Figure 6, it was found that the drag force term in Equation 4 could be written as

$$D_i u_i |\vec{u}|^{s_i} \qquad i = 1, 2, 3 \tag{10}$$

where D_i is independent of $|\vec{u}|$ and the values of s_i were 0.85, 0.86, and 0.87 for axes 1, 2, and 3 respectively. Comparing Equations 4 and 10, one sees that the dependence of the drag coefficient on the magnitude of the velocity $|\vec{u}|$ was

$$C_D \propto |\vec{u}|^{s_i - 1} \simeq |\vec{u}|^{-0.14} \tag{11}$$

Thus, in the velocity region of the calibration from 20 cm-sec^{-1} to 110 cm-sec^{-1}, the drag coefficient showed a decrease with increasing velocity. If the calibration Reynolds number is defined as $|\vec{u}| 2r/\nu$ where r is the radius of the outer sphere and ν is the kinematic viscosity of water, the calibration Reynolds number ranged from 2×10^4 to 1×10^5.

Using Equation 10 for the drag force term in Equation 4, one obtains

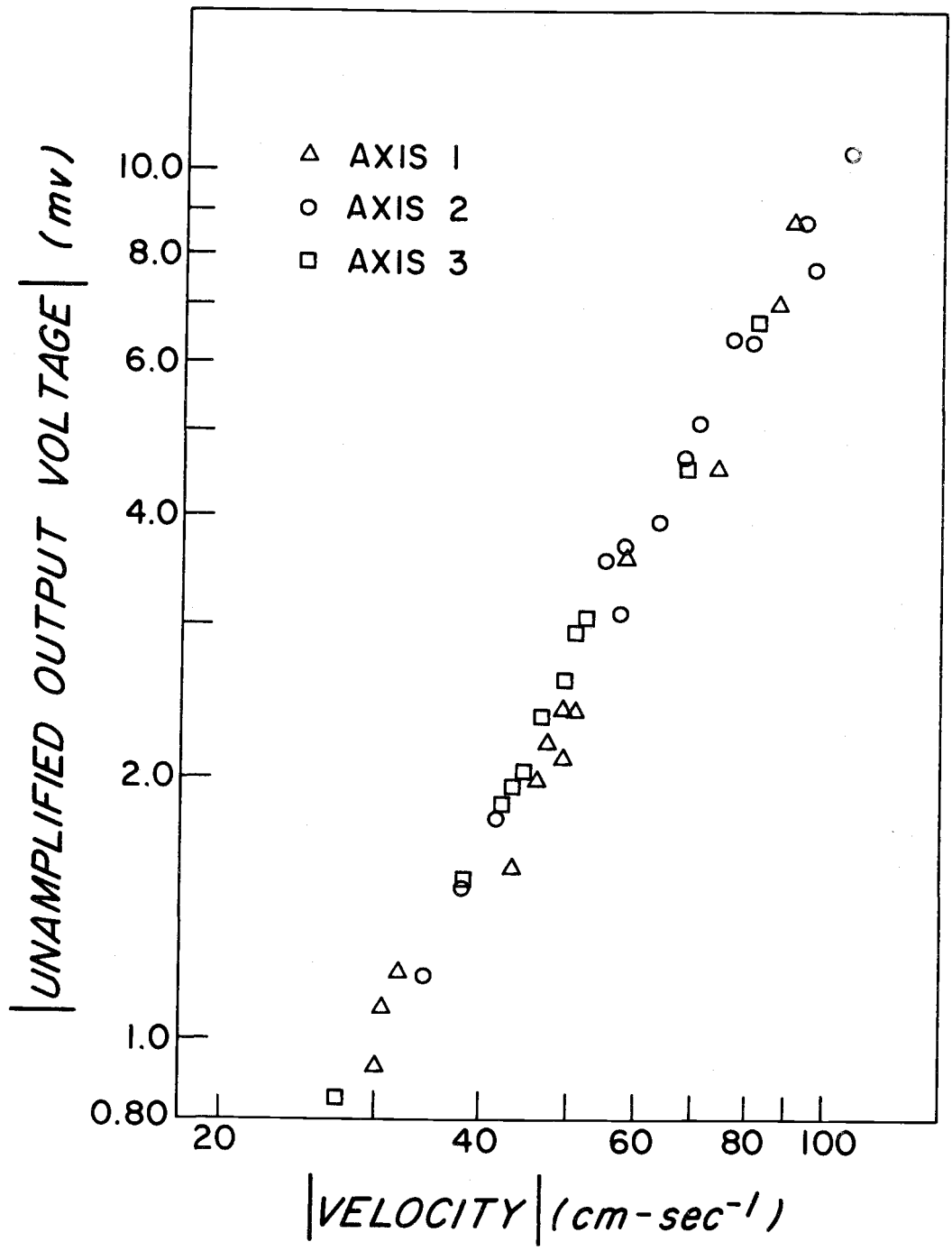

Figure 6. Drag probe response to water velocity.

$$E_i - e_i = D_i u_i |\vec{u}|^{s_i} + H_i \frac{du_i}{dt} \qquad i = 1, 2, 3 \qquad (12)$$

At time points where the velocity was not entirely along one axis and where neither term in Equation 12 was negligible compared to the other, Equation 12 was used to verify that the theoretical outputs agreed with the observed outputs.

The magnitudes of each D_i and H_i depend upon the spring constants of the compressed sponge rubber, the gain settings of the operational amplifiers in the probe circuit, and the gain settings of any external amplifiers which are used. When the water velocities and accelerations were in c.g.s. units, the ratios D_i/H_i for the three axes were 0.082, 0.099, and 0.116. These ratios are later used to investigate the relative importance of the drag and inertial terms in Equation 12 and in a numerical technique to obtain three velocity components from drag probe measurements of three force components. The differences in the ratios for each axis were possibly due to the nonspherical shape of the outer sphere and to the resilient behavior of the sponge rubber supports.

The primary source of error in the calibration procedure was the mathematical determination of the water velocity and the water acceleration from records of the pendulum displacements. These errors are estimated to be ±5% and, because the drag probe was

calibrated twice with consistent results, the calibration appears to be good to ±5%.

Among investigators who have measured wave forces exerted on objects there is some controversy about the dependence of the drag and inertial coefficients upon various parameters. As an example, Keulegan and Carpenter (1958) measured the forces exerted on cylinders and flat plates subjected to standing waves in a wave tank and found that the drag and inertia coefficients depended upon the dimensionless parameter $u_{MAX}T/2r$. u_{MAX} is the maximum value of the wave particle velocity, T is the wave period, and r is the radius of the cylinder or plate. From the drag probe calibrations, it was found that the drag coefficient C_D depended only on $|\vec{u}|$ and not on $u_{MAX}T/2r$ where r is the radius of the outer sphere. The inertial coefficient C_M was independent of $|\vec{u}|$ and $u_{MAX}T/2r$. If the calibration Reynolds number is defined as $|\vec{u}|2r/\nu$ where ν is the kinematic viscosity of water, C_D was a function of the Reynolds number and C_M was independent of the Reynolds number. The same results were obtained by O'Brien and Morison (1952) in their study of wave forces exerted on a sphere in a wave tank.

III. TECHNIQUES TO OBTAIN VELOCITY COMPONENTS FROM DRAG PROBE MEASUREMENTS

Equation 12 which relates the drag probe voltage outputs to the water velocity and acceleration describes a set of three coupled non-linear differential equations. It is thus difficult to obtain the desired velocity components from the measured force components.

Interpretation of Drag Probe Measurements

Use of the Drag Probe Beneath Surface Gravity Waves

The total derivative in Equation 12 can be written as

$$\frac{du_i}{dt} = \frac{\partial u_i}{\partial t} + u_1 \frac{\partial u_i}{\partial x_1} + u_2 \frac{\partial u_i}{\partial x_2} + u_3 \frac{\partial u_i}{\partial x_3} \qquad i = 1,2,3 \qquad (13)$$

To determine the relative magnitudes of the terms in Equation 12, let us consider a single Fourier component of the wave velocity

$$u = a\sigma \cos(kx-\sigma t) \qquad (14)$$

where a is the wave amplitude in cm, k is the wave number (2π/wavelength in cm), and σ is the radian frequency, $2\pi f$. The terms in Equation 12 may thus be written as

$$Du|u|^s \simeq Du|u| = Da^2\sigma^2 \cos(kx-\sigma t)|\cos(kx-\sigma t)| \qquad (15)$$

$$H \frac{\partial u}{\partial t} = -Ha\sigma^2 \sin(kx-\sigma t) \tag{16}$$

$$Hu \frac{\partial u}{\partial x} = -Ha^2\sigma^2 k \cos(kx-\sigma t) \sin(kx-\sigma t) \tag{17}$$

To simplify the algebra, s has been approximated by unity instead of the actual value of about 0.86.

From Equations 16 and 17, the ratio of the nonlinear convective acceleration force term to the local acceleration force term is $ak \cos(kx-\sigma t)$. The maximum value of ak as determined from conditions for wave breaking is 0.547 (Michell, 1893). In general ak is much smaller (typically 0.1) and one is able to use "linear" wave theory. The total acceleration du_i/dt is then almost entirely determined by $\partial u_i/\partial t$, the local particle acceleration. As an example, the value of ak for a wave 100 cm in amplitude with a frequency of 0.1 Hz is about 0.04.

From Equations 15 and 16 the ratio of the local acceleration force term to the drag force term is

$$\frac{-H \sin(kx-\sigma t)}{aD \cos(kx-\sigma t) \left| \cos(kx-\sigma t) \right|} = \frac{-10 \sin(kx-\sigma t)}{a \cos(kx-\sigma t) \left| \cos(kx-\sigma t) \right|} \tag{18}$$

The ratio H/D has been approximated by the value of about 10 obtained in the drag probe calibration. After approximating s by unity in Equation 15, H/D is in units of length and the value of 10 in Equation 18 has units of cm. Equation 18 shows that the local

acceleration contribution to the inertial force is not always negligible in comparison to the drag force. If a is large, however, the local acceleration contribution is small in comparison to the drag force except near velocity zero crossings when $\cos(kx-\sigma t) = 0$. Note also, at velocity zero crossings, the nonlinear convective contributions are zero and the local acceleration determines the force exerted on the drag probe.

Hence, beneath waves, an accurate approximation for Equation 12 is

$$E_i - e_i \simeq D_i u_i |\vec{u}|^{s_i} + H_i \frac{\partial u_i}{\partial t} \qquad i = 1, 2, 3 \qquad (19)$$

Use of the Drag Probe to Measure Turbulence

For turbulence measurements, the response of the drag probe is limited by the finite size of the sensing head. Assuming that the turbulence is "frozen" into the mean flow U, one can use Taylor's hypothesis, $k = 2\pi f/U$ to relate the frequency f in Hz to the wave number k of the turbulence. Away from a boundary, Taylor's hypothesis is valid when the mean velocity is much larger than the turbulent velocity fluctuations (see, for example, Hinze, 1959, p. 40). Averaging a velocity Fourier component $u \cos(Ukt)$ over the surface of a sphere of radius r yields (Smith, 1966)

$$\bar{u} = u \cos(Ukt) \frac{\sin(kr)}{kr} \tag{20}$$

in which $\bar{u}$ is the average velocity. At the 3 db point, $\sin(kr)/kr$ is 0.707 and kr is 1.39. For $r = 5$ cm, the drag probe response will be greater than 3 db down for length scales shorter than 22 cm. The drag probe frequency response is not limiting because a mean velocity greater than 616 cm-sec^{-1} is required for an eddy of length scale 22 cm to have an apparent frequency greater than 28 Hz, the frequency at which the probe response is 3 db down.

To make further use of Taylor's hypothesis, let the velocity components of u be given by

$$u_1 = U + u_{1t} \tag{21}$$

$$u_2 = u_{2t} \tag{22}$$

$$u_3 = u_{3t} \tag{23}$$

where U is the mean velocity and u_{1t}, u_{2t}, and u_{3t} are the fluctuating turbulent velocity components. When Taylor's hypothesis is valid

$$\frac{\partial u_i}{\partial t} \simeq -U \frac{\partial u_{it}}{\partial x_1} \qquad i = 1, 2, 3 \tag{24}$$

and

$$\frac{du_i}{dt} \simeq \left(\frac{\partial u_i}{\partial t} + U \frac{\partial u_{it}}{\partial x_1}\right) \simeq 0 \qquad i = 1, 2, 3 \tag{25}$$

Equation 24 states that the local acceleration is due to the convection of velocity gradients past the observer by the mean flow. From Equation 25, the total derivative is small and Equation 12 becomes

$$E_i - e_i \simeq D_i u_i |\vec{u}|^{s_i} \qquad i = 1, 2, 3 \tag{26}$$

Equation 26 is a set of three coupled algebraic equations which are easily solved for the velocity components.

If a time varying nonturbulent flow is also present and the velocities u_{iN} associated with this flow are much larger than the turbulent velocities u_{it}, the turbulence may be "frozen" into the vector sum of the nonturbulent time varying flow and the mean flow. Equation 12 thus becomes

$$E_i - e_i \simeq D_i u_i |\vec{u}|^{s_i} + H_i \frac{\partial u_{iN}}{\partial t} \qquad i = 1, 2, 3 \tag{27}$$

where u_{iN} is the ith component of the nonturbulent time varying flow and the velocity components u_i of $\vec{u}$ include the mean velocity, the time varying nonturbulent flow, and the turbulent velocity fluctuations. To obtain Equation 27 it is assumed that the convective terms associated with the nonturbulent time varying flow are

negligible in comparison to the other terms in Equation 12. Such a situation would exist, for example, if the nonturbulent flow were due to velocities associated with surface gravity waves. Because there is no way to a priori separate turbulent and nonturbulent contributions to the forces measured by the drag probe, Equation 27 may be approximated by

$$E_i - e_i \simeq D_i u_i |\vec{u}|^{s_i} + H_i \frac{\partial}{\partial t}(u_{iN} + u_{it}) \tag{28}$$

The numerical technique to be described can then be used to obtain the velocity components. The solutions obtained will only be accurate estimates of the actual velocity components u_i when the additional term $\partial u_{it}/\partial t$ in Equation 28 is negligible in comparison to the other terms in the equation. If the mean flow is sufficiently large so that the drag force term in Equation 28 never becomes zero, the numerical technique should yield accurate estimates. Except near velocity zero crossings, Equation 28 will yield good results. Thus, the essential assumption in using the drag probe to measure turbulence is that the error introduced by the additional term $\partial u_{it}/\partial t$ is negligible.

A Numerical Technique to Obtain the Velocity Components

As we have seen the inertial term in Equation 12 cannot always

be neglected in comparison to the drag term. However, the nonlinear convective contributions to the inertial term may often be neglected and we obtained the following equation

$$E_i - e_i = D_i u_i |\vec{u}|^{s_i} + H_i \frac{\partial u_i}{\partial t} \qquad i = 1, 2, 3 \tag{29}$$

Equation 29 is the same as Equation 19 and 28. An analytical solution to Equation 29 has not been found but the equation can be readily solved by several numerical predictor corrector methods. Using the drag probe in the field, one does not know the velocity components at any time and, hence, initial conditions cannot be prescribed. This problem is avoided by selecting arbitrary initial values and running the numerical solution to Equation 29 until velocity values are obtained which are independent of the initial values. In essence, a quasi-steady-state solution is obtained and such a solution is independent of the initial conditions.

There are numerous predictor corrector methods and one generally chooses the simplest method which yields acceptable accuracy. Predictor corrector methods are derived from Taylor series expansions and the primary source of error in solving Equation 29 by predictor corrector techniques is the truncation error due to neglecting higher order terms in the Taylor series expansions. Truncation errors are of the form

$$\frac{\Delta t^m u^{(m)}_{iMAX}}{m!} \tag{30}$$

where Δt is the time interval between the points at which the solution is determined, $u^{(m)}_{iMAX}$ is the maximum value of the mth derivative of u_i, and m depends on the predictor corrector technique which is used (see, for example, Hamming, 1965). To determine which predictor corrector technique to use, one can examine the relative truncation error

$$\frac{\dfrac{\Delta t^m u^{(m)}_{iMAX}}{m!} - \dfrac{(\Delta t)^{m+1} u^{(m+1)}_{iMAX}}{(m+1)!}}{\dfrac{\Delta t^{(m)} u^{(m)}_{iMAX}}{m!}} \tag{31}$$

The size of Expression 31 determines whether it is worthwhile to use a more complicated predictor corrector technique. As an example, for the data which is used in this thesis, $\Delta t = 0.1$ sec, $m = 3$, and primary contributions to the third and fourth derivatives are from frequencies near the folding (Nyquist) frequency 5 Hz. Considering a single Fourier component $u \cos(\sigma t)$ where $\sigma = 31.4$ radians-sec^{-1}, the value of Expression 31 is 0.21 and a 21% decrease in truncation error can be obtained by using a predictor-corrector technique with $m = 4$. Expression 30 has a value of about 10 u and, since u at $\sigma = 31.4$ radians-sec^{-1} is less than 0.001 of the primary velocity

contributions, the truncation error is about 1% of the primary velocity contributions. Thus, the technique which is described below is adequate and it is probably not worthwhile to use a more complicated method. As a predictor corrector method is run on a computer, one may use the difference between the predictor and the corrector at each time step as an estimate of the truncation error. If the truncation error is too large, a smaller time step Δt or a more complicated predictor corrector technique may be required. For the data in this thesis, the truncation errors as estimated from the differences between the predictor and corrector values were generally less than 1% of the computed velocity values.

A simple predictor corrector technique can be developed from a Taylor series expansion for each u_i. Let $u_{in} = u_i(n\Delta t)$ and $u'_{in} = u'_i(n\Delta t)$ where Δt is a time interval.

$$u_{i(n+1)} = C_{i(n+1)} + \frac{1}{5}[P_{i(n+1)} - C_{i(n+1)}] \tag{32}$$

where

$$P_{i(n+1)} = u_{i(n-1)} + 2\Delta t u'_{in} \tag{33}$$

$$C_{i(n+1)} = u_{in} + \frac{\Delta t}{2}[u'_{i(n+1)} + u'_{in}] \tag{34}$$

$P_{i(n+1)}$ is called a predictor for $u_{i(n+1)}$ and $C_{i(n+1)}$ is called a corrector for $u_{i(n+1)}$. Using Equation 29 and $P_{i(n+1)}$ for $u_{i(n+1)}$, one can obtain the relation between $P_{i(n+1)}$ and

$u'_{in} = \partial u_i(n\Delta t)/\partial t$

$$u'_{i(n+1)} = \frac{E_i - e_i}{H_i} - \frac{D_i}{H_i} P_{i(n+1)} \left[\sum_{i=1}^{3} P^2_{i(n+1)} \right]^{s_i/2} \tag{35}$$

To begin the numerical procedure, arbitrary initial values u_{i0}, u_{i1}, and u'_{i1} are prescribed. Equation 33 is solved for P_{i2}, Equation 35 is solved for u'_{i2}, Equation 34 is solved for C_{i2}, and Equation 32 is solved for u_{i2}. Using u_{i2} as a better predicted value, P_{i2}, this procedure is repeated once more to obtain more accurate estimates for u'_{i2} and u_{i2}. The process just described is then continued as one iterates (increments n) to the end of a given data record.

One can determine the value of n for which the computed velocity components are independent of several sets of arbitrary initial conditions and can throw away the velocity values before this point. If one has a short record, the following equations may be used to extend the solution backward from the point where the initial conditions no longer affect the velocity values.

$$u_{i(n-1)} = C_{i(n-1)} + \frac{1}{5}\left[P_{i(n-1)} - C_{i(n-1)}\right] \tag{36}$$

where

$$P_{i(n-1)} = u_{i(n+1)} - 2\Delta t u'_{in} \tag{37}$$

$$C_{i(n-1)} = u_{in} - \frac{\Delta t}{2}[u'_{in} + u'_{i(n-1)}] \tag{38}$$

The predictor corrector scheme that has been described was tested on numerous sets of generated data. From assumed velocity records, force records were generated and the predictor corrector scheme was used to obtain computed velocity values for comparison to the known values. Table 1 shows the results of a typical test. Each s_i in Equation 30 was 0.86 and the ratios D_i/H_i were 0.082, 0.099, and 0.116. These values were the values obtained from the drag probe calibration. The computed velocities converge to the actual velocities within about 100 steps (5 seconds) which is less than two wave periods.

Table 1. Test of numerical procedure applied to forces produced by a mean flow and wave type velocities ($u_1 = 5.00 + 17.30 \cos(2.00\, n\Delta t)$, $u_2 = 10.00 \cos(2.00\, N\Delta t)$, $u_3 = 20.00 \sin(2.00\, n\Delta t)$, $\Delta t = 0.05$ sec).

n	u_1 (cm-sec^{-1}) Actual	u_1 (cm-sec^{-1}) Computed	u_2 (cm-sec^{-1}) Actual	u_2 (cm-sec^{-1}) Computed	u_3 (cm-sec^{-1}) Actual	u_3 (cm-sec^{-1}) Computed
0	22.30	0	10.00	0	0	0
1	22.23	.63	9.95	.28	2.00	.86
2	21.98	2.28	9.80	.98	3.97	3.28
5	20.20	5.04	8.78	1.97	9.59	9.81
10	14.36	4.44	5.40	.89	16.83	18.25
15	6.23	-.67	.71	-2.45	19.95	21.25
20	-2.21	-7.09	-4.16	-6.35	18.19	18.74
25	-8.88	-12.20	-8.01	-9.39	11.97	11.91
30	-12.15	-14.27	-9.90	-10.64	2.82	2.57
40	-6.32	-7.22	-6.54	-6.72	-15.14	-15.14
50	9.91	9.46	2.84	2.75	-19.18	-19.19
60	21.63	21.47	9.60	9.58	-5.59	-5.65
80	2.48	2.47	-1.46	-1.45	19.79	19.78
100	-9.53	-9.54	-8.39	-8.39	-10.88	-10.88
200	12.07	12.07	4.08	4.08	18.26	18.26
500	21.71	21.71	9.65	9.65	-5.25	-5.25

IV. THEORY APPLICABLE TO THE MEASUREMENTS

Linear Wave Theory and Wave Statistics

The sea surface deformation and the subsurface pressure and velocity fields due to waves are exceedingly complicated and can be considered to consist of many sinusoidal components of different frequencies, amplitudes, phases, and directions. Nonlinear effects are of order ak and, if ak is small, the wave surface in two dimensions may be described by

$$\eta(\vec{x}, t) = \sum_n a_n \cos(\vec{k}_n \cdot \vec{x} - \sigma_n t + \epsilon_n) \tag{39}$$

where $\vec{x} = (x, y)$ is the position in a horizontal plane, σ_n is a radian frequency, $\vec{k}_n = (k_n \cos\theta_n, k_n \sin\theta_n)$, $k_n = |\vec{k}_n|$ and $\vec{k}_n$ indicates the propagation direction in the x, y plane. The phases, ϵ_n, are assumed to be uniformly randomly distributed over $(0, 2\pi)$ and the surface is considered to be a statistical ensemble of surfaces.

If the motion is irrotational and the water is incompressible, the velocity potential ϕ must satisfy Laplace's equation

$$\nabla^2 \phi = 0 \tag{40}$$

The velocity u is obtained from the velocity potential

$$\vec{u} = \nabla \phi \tag{41}$$

In deep water of depth d where kd is large ($kd > 3$), a solution to Laplace's equation which satisfies the linearized surface kinematic and dynamic boundary conditions corresponding to Equation 39 and the requirement that the velocity vanish as the depth approaches infinity is

$$\phi(x, y, z, t) = \sum_n \frac{a_n \sigma_n}{k_n} e^{k_n z} \sin(\vec{k}_n \cdot \vec{x} - \sigma_n t + \epsilon_n) \tag{42}$$

in which z is positive upwards and is zero at the undisturbed surface. The wave number magnitudes k_n and the radian frequencies σ_n are related by

$$\sigma_n^2 = g k_n \tag{43}$$

where g is the acceleration due to gravity.

From Equations 41 and 42 one obtains the velocity components

$$u = \sum_n a_n \sigma_n \cos\theta_n e^{k_n z} \cos(\vec{k}_n \cdot \vec{x} - \sigma_n t + \epsilon_n) \tag{44}$$

$$v = \sum_n a_n \sigma_n \sin\theta_n e^{k_n z} \cos(\vec{k}_n \cdot \vec{x} - \sigma_n t + \epsilon_n) \tag{45}$$

$$w = \sum_n a_n \sigma_n e^{k_n z} \sin(\vec{k}_n \cdot \vec{x} - \sigma_n t + \epsilon_n) \tag{46}$$

where u, v, and w are in the x, y, and z directions respectively.

From Bernoulli's equation, one obtains the subsurface pressure

$$p = \rho g \sum_n a_n e^{k_n z} \cos(\vec{k}_n \cdot \vec{x} - \sigma_n t + \epsilon_n) \tag{47}$$

In the limit as the number of terms in Equation 39 approaches infinity, we suppose that the frequencies are densely distributed in $(0, \infty)$. Letting $\psi(f, \theta)dfd\theta$ be the contribution to the mean square value of w from frequencies in the range $(f - \frac{df}{2}, f + \frac{df}{2})$ and directions in the range $(\theta - \frac{d\theta}{2}, \theta + \frac{d\theta}{2})$, one obtains the following spectral relations from Equations 44 through 47.

$$C_{ww}(f) = \int_0^{2\pi} \psi(f, \theta)d\theta \tag{48}$$

$$C_{uu}(f) = \int_0^{2\pi} \cos^2\theta\psi(f, \theta)d\theta \tag{49}$$

$$C_{vv}(f) = \int_0^{2\pi} \sin^2\theta\psi(f, \theta)d\theta \tag{50}$$

$$Q_{uw}(f) = \int_0^{2\pi} \cos\,\theta\psi(f,\theta)d\theta \tag{51}$$

$$Q_{vw}(f) = \int_0^{2\pi} \sin\,\theta\psi(f,\theta)d\theta \tag{52}$$

$$C_{uw}(f) = 0 = C_{vw}(f) \tag{53}$$

$$C_{ww}(f) = C_{uu}(f) + C_{vv}(f) \tag{54}$$

$$\rho^2 g^2 C_{ww}(f) = 4\pi^2 f^2 C_{pp}(f) \tag{55}$$

where C_{ij} is the cospectrum between the time series i and j and Q_{ij} in the quadrature spectrum between the time series i and j.

The coherence squared values between the vertical velocity component and the horizontal velocity components are

$$\gamma_{uw}^2 = \frac{\left[\int_0^{2\pi} \psi(f,\theta)\cos\,\theta\,d\theta\right]^2}{\int_0^{2\pi} \psi(f,\theta)d\theta \int_0^{2\pi} \psi(f,\theta)\cos^2\theta d\theta} \tag{56}$$

$$\gamma_{vw}^2 = \frac{\left[\int_0^{2\pi} \psi(f,\theta)\sin\,\theta\,d\theta\right]^2}{\int_0^{2\pi} \psi(f,\theta)d\theta \int_0^{2\pi} \psi(f,\theta)\sin^2\theta\,d\theta} \tag{57}$$

From measurements of the velocity components, one can obtain the first five Fourier coefficients for the Fourier series expansion of $\psi(f, \theta)$ as a function of θ

$$\psi(f, \theta) \simeq \frac{a_0}{2} + a_1 \cos \theta + \beta_1 \sin \theta + a_2 \cos 2\theta + \beta_2 \sin 2\theta \qquad (58)$$

Because Equation 58 can have negative values, Lonquet-Higgins (1962) introduced the following alternate approximation

$$\psi(f, \theta) \simeq \frac{a_0}{2} + \frac{2}{3}(a_1 \cos \theta + \beta_1 \sin \theta) + \frac{1}{6}(a_2 \cos 2\theta + \beta_2 \sin 2\theta) \qquad (59)$$

$\psi(f, \theta)$ is power preserving and integrating Equation 58 or 59 over $(0, 2\pi)$ yields the frequency energy spectrum for w. Because $\psi(f, \theta)$ contains only five coefficients it is a strongly smoothed version of the actual directional spectrum. The smoothing effect is later illustrated in the discussion of drag probe measurements beneath ocean waves. The values of the Fourier coefficients are obtained from the following equations

$$a_0 = \frac{1}{\pi} C_{ww}(f) \qquad (60)$$

$$a_1 = \frac{1}{\pi} Q_{uw}(f) \qquad (61)$$

$$\beta_1 = \frac{1}{\pi} Q_{vw}(f) \qquad (62)$$

$$\alpha_2 = \frac{1}{\pi}[C_{uu}(f) - C_{vv}(f)] \tag{63}$$

$$\beta_2 = \frac{2}{\pi} C_{uv}(f) \tag{64}$$

Turbulence Theory

Let us assume that there is a steady mean current and let us align a right-handed coordinate system so that the x direction is positive in the down-stream direction, the y direction is in the cross-stream direction, and the z direction is positive upwards. Dividing the velocity field into its mean and fluctuating parts, we may thus write

$$\vec{u}(x, y, z, t) = U + u_{1t}(t), u_{2t}(t), u_{3t}(t)) \tag{65}$$

in which U is the mean current and u_{1t}, u_{2t} and u_{3t} are the components of the fluctuating velocity field. From time records of the velocity components, one can obtain the usual energy spectra and the cross-spectra.

If the turbulence is being moved past the measurement point by the mean velocity, Taylor's hypothesis $k = 2\pi f/U$ can be used to relate frequencies in Hz to the wave numbers k. Theoretically, if one is near a boundary, the larger scale eddies are distorted and thus Taylor's hypothesis requires that $kz \gg 1$ where z is the

distance from the boundary.

It can be shown that (see, for example, Hinze, 1959), for a sufficiently large mean flow Reynolds number, a locally isotropic region known as the inertial subrange is likely to exist at high wave numbers and that the downstream wave number spectrum $\Phi(k)$ in this region depends only on $\overline{\epsilon}$, the average rate of dissipation of turbulent kinetic energy per unit mass, and the wave number k. Near a boundary, the mean flow Reynolds number may be taken as Uz/ν where z is the distance from the boundary and ν is the kinematic viscosity of the fluid. $\Phi(k)dk$ is the contribution to the time averaged value of u_{1t}^2 from wave numbers in the range $(k-\frac{dk}{2}, k+\frac{dk}{2})$. In the inertial subrange, dimensional analysis shows $\Phi(k)$ to be of the form

$$\Phi(k) = K'\overline{\epsilon}^{2/3}k^{-5/3} \tag{66}$$

where K' is a universal constant. In the inertial subrange, the vertical and cross stream wave number spectra are also proportional to $k^{-5/3}$. If Taylor's hypothesis is used, all of the spectra are proportional to $f^{-5/3}$. Theoretically, if the flow is to be isotropic, we must require that $kz \gg 1$ when making measurements near a boundary. Numerous measurements, however, have indicated that a $k^{-5/3}$ region extends to low wave numbers (particularly for the u_{1t} component) where kz is not large compared to unity.

The Reynolds stresses are given by

$$\tau_{ij} = -\rho\overline{u_i u_j} \tag{67}$$

where ρ is the fluid density and the overbar indicates a time average, τ_{ij} can be interpreted as the flux of j directed momentum which is transported in the i direction. The units for the Reynolds stresses are momentum/(area x time).

V. VELOCITY MEASUREMENTS BENEATH DEEP WATER OCEAN WAVES

Description of Experiment

On May 3, 1970, measurements of wave orbital velocities and wave pressure were made from the TOTEM buoy 30 mi off the Oregon coast. The TOTEM buoy which is described by Neshyba et al. (1970) is a large moored spar buoy with a length of 55 m and a diameter of 1.1 m. The water depth was 550 m and thus all waves were deep water waves. To the writer's knowledge, these are the first direct measurements of wave orbital velocities in the open ocean. Figure 7 shows the experimental arrangement during the measurements. Signals were sent via a floating cable to the R/V CAYUSE which maintained station about 100 m from the TOTEM buoy.

The pressure sensor (Ocean Engineering Corporation Model PT-404) was a balanced strain gauge Wheatstone bridge device with a slow leak so that very low frequency pressures and mean pressures were not detected.

Data Collection and Processing

Before being recorded on a Hewlett-Packard Model 3955 analog tape recorder, all signals were passed through inverting Nexus SQ-10a operational amplifier circuits with simple RC low pass filters

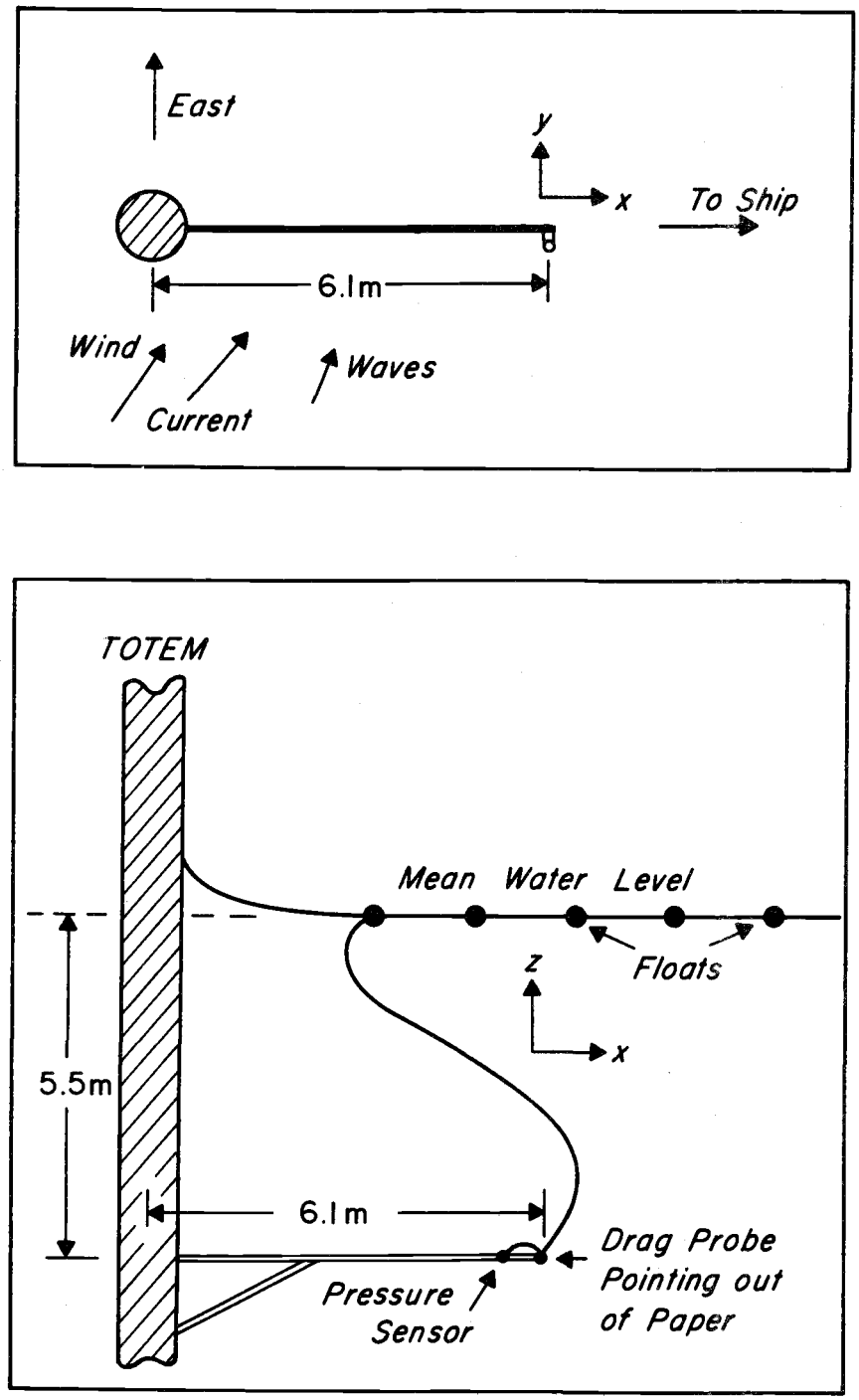

Figure 7. TOTEM experimental arrangement.

(3 db point 16 Hz). The amplifiers were used to remove high frequency noise and to amplify the signals. With an offset control, the mean drag probe voltages were removed so that the full range of the tape recorder ±1.4 V could be used. So that mean velocity components could be determined, the voltage offsets were recorded and, after the drag probe was retrieved, the mean voltage outputs were measured at zero velocity. A spring scale was then used to check the drag probe's response to static forces. This static force data is plotted in Figure 3.

The analog tape was digitized with equipment belonging to the Institute of Oceanography at the University of British Columbia. During digitizing all signals were amplified by Fairchild μA741 operational amplifiers so that any added digital noise was negligible. A sampling rate of 0.10 sec was used and the digital values were recorded on incremental magnetic tape.

For drag probe data, the velocity components were obtained from the force components by the predictor corrector technique that has been described. The s_i values for the three axes were 0.85, 0.86, and 0.87 and the ratios D_i/H_i were 0.082, 0.099, and 0.116 for the three axes. After the velocity components were obtained, a fast Fourier transform program available from the Oregon State University Computer Center was used to obtain the Fourier coefficients of the digitized velocity records and the digitized pressure

record. All spectral computations were performed with a CDC-3300 computer at the Oregon State University Computer Center. Simpler computations were performed with a DEC PDP-8S computer in the Oceanography Department.

To study the variation of the final spectral estimates, each record was broken into several files and each file was separately transformed. From the Fourier coefficients of two simultaneous time series, the energy spectrum for each series, the cospectrum, and the quadrature spectrum were determined. A band averaging technique was chosen to make the spectral estimates almost equally spaced when plotted versus the logarithm of the frequency. The bands are centered about the frequency given in Table 2 and the bandwidth is the number of degrees of freedom given in Table 2 divided by twice the record length. The energy spectra, the cospectrum and the quadrature spectrum were averaged within each band for each file and were then averaged over the corresponding bands for the entire record. From the observed standard deviations of the spectral estimates over the total number of files making up a record, one can obtain the equivalent degrees of freedom as defined by Blackman and Tukey (1958, p. 22). Because the observed degrees of freedom did not differ greatly from the theoretical values (twice the number of Fourier coefficients in a band) only the latter degrees of freedom are given in Table 2. Thus, for waves, it appears that the degrees of freedom

TABLE 2. Spectral Results for Wave Data

Frequency Hz	C_{pp} (cm^2-sec)	Degrees of Freedom	C_{ww} (cm^2-sec^{-1})	C_{uu} (cm^2-sec^{-1})	C_{vv} (cm^2-sec^{-1})	Degrees of Freedom	θ_{uw} (°)	θ_{vw} (°)	γ^2_{uw}	γ^2_{vw}
.0537	568	112	1199	1603	1470	48	6	102	.005	.083
.0732	1855	112	1460	1197	1296	48	211	70	.041	.307
.0928	2520	112	1042	798	985	48	14	100	.015	.254
.1123	2710	112	1481	902	1230	48	31	83	.114	.524
.1416	1452	224	1551	724	957	96	60	74	.065	.510
.1807	1140	224	1502	507	777	96	15	69	.063	.093
.2197	329	224	737	431	346	96	100	81	.019	.068
.2588	108	224	323	312	212	96	112	93	.017	.032
.3174	23.7	448	118	170	143	192	250	103	.040	.002
.3955	3.52	448	54.9	160	96.9	192	335	124	.0003	.033
.4736	1.57	448	29.0	134	51.9	192	148	158	.005	.003
.5518	1.18	448	19.7	95.9	39.2	192	11	74	.001	.020
.6690	.768	896	10.2	72.1	25.6	384	330	196	.007	.001
.8252	.553	896	4.63	51.6	11.2	384	356	23	.040	.005
.9815	.413	896	2.03	53.2	6.37	384	34	201	.024	.004

concept is useful in estimating variability of the spectral estimates. From the averaged cospectrum and quadrature spectrum values, the phase and coherence squared were computed.

Results

The results to be discussed are presented to indicate that a drag probe is a suitable instrument to measure wave velocities. Errors may be introduced by the hysteresis and crosstalk of the drag probe, by one axis of the drag probe not being exactly vertical, by wave reflection from TOTEM, and by motion of TOTEM. Possible errors due to not aligning with the vertical are computed from the standard equations for the rotation of a rectangular coordinate system. The effect is to mix the horizontal and vertical velocity components. For tilts up to 8° it is estimated that the vertical and horizontal velocity cospectra can be in error by 7% of the actual vertical velocity energy spectrum. By applying the equations developed by Morse (1936, p. 347) for sound wave reflection from a vertical cylinder to the velocity potential for surface gravity waves, one can show that the reflected wave amplitude due to TOTEM must be less than 4% of the incident wave amplitude throughout the wave frequency band. If reflected waves are present, the cospectra between the vertical wave velocity and the horizontal wave velocities need not be zero. The heave resonant frequency for TOTEM is 0.045 Hz and the pitch resonant

frequency is 0.027 Hz (Nath and Neshyba, 1970). In addition, very slight motions of the buoy can cause much larger velocities and accelerations at the end of the support to which the drag probe is attached. The cumulative effect of the above errors is difficult to determine but could be as large as 20%.

A 48 minute pressure record and a 21 minute drag probe record have been analyzed. Unfortunately, the records were not simultaneous. The pressure record ended approximately 90 minutes before the force record began. During the pressure record, the drag probe in use was not operating correctly. Divers replaced the probe with the one that has been described in this thesis and recording was continued. A chart recorder was not available for the cruise and it was difficult to tell whether the sensors were performing normally. Prior to the installation of the second drag probe, the pressure record had developed spurious low frequency noise. The source of this noise is not known but is believed due to a poor connection between the floating cable and the R/V CAYUSE. The cable had to be disconnected from the ship several times when the ship was unable to stay close enough to the TOTEM buoy. During the data analysis, an attempt was made to correct that portion of the pressure spectrum which was simultaneous with the force record. Because the noise contaminated the pressure record at wave frequencies in a peculiar manner, this correction was unsuccessful.

The wind speed was measured approximately every 10 minutes with the ship's cup anemometer and was an almost steady 6 $m\text{-}sec^{-1}$. The prevailing wind direction and the apparent direction of the dominant waves are shown in Figure 7. There was almost no wave breaking and the sea was quite shortcrested. During the 24 hr period before the measurements, the wind speed was generally between 10 $m\text{-}sec^{-1}$ and 20 $m\text{-}sec^{-1}$. The mean current, as determined from the drag probe, was 20 $cm\text{-}sec^{-1}$ in the direction shown in Figure 7. Because the zero velocity output of the probe could only be obtained after the probe was retrieved and returned to the ship the mean velocity magnitude may be in error by perhaps 25%. The mean velocity direction is believed correct to within ±45°.

The wave velocities and the wave pressure described by Equations 44 through 47 are thought to be sums of independent random variables and, by the central limit theorem, should have normal probability distributions as the number of terms in the sums becomes large. Figure 8 is a plot of the cumulative probability distributions of the pressure record and the vertical velocity record on normal probability paper. The straight lines represent the normal curves corresponding to the observed root mean square wave pressure, 17.2 cm of water, and the observed root mean square vertical velocity, 19.3 $cm\text{-}sec^{-1}$. The pressure given by Equation 47 has been normalized by dividing by ρg. Figure 8 indicates that the wave

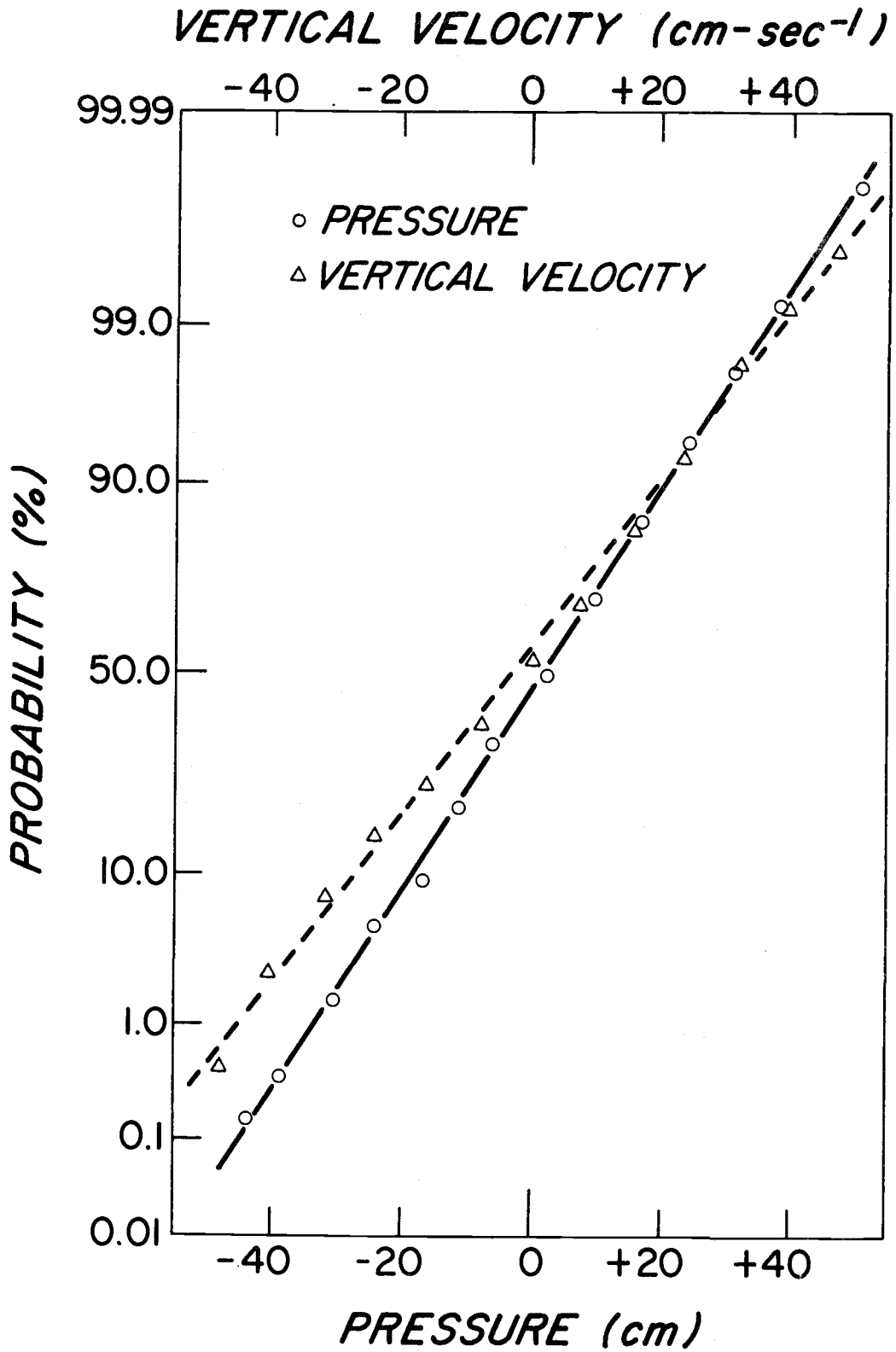

Figure 8. Vertical velocity and pressure cumulative probability distributions.

pressure and vertical velocity have probability distributions that are nearly normal.

Table 2 is a summary of the statistical results. The low frequency portions of the velocity spectra may be too large because of TOTEM motion and the drag probe hysteresis. Figure 9 shows the logarithms of the energy spectra plotted vs the logarithm of the frequency. The line drawn in Figure 9 is a reference line only and has a slope of -3. The u spectrum does not drop as rapidly as either the v or w spectrum and, since it is unlikely that any real turbulence would only appear in the u spectrum, we must consider the u spectrum to be noisy at high frequencies. Because the noise was not seen in calibrations before and after the cruise, its source is unknown. It may perhaps be due to eddy shedding from the drag probe outer sphere. The fact that the noise does not occur in the v and w spectra indicates that the three equations described by Equation 19 are relatively uncoupled for this set of measurements. If the wave velocity magnitude is very slowly varying and $|\vec{u}|$ is primarily determined by the mean velocity and the wave velocity, then $|\vec{u}|$ may be approximately constant and Equation 19 becomes three separate linear partial differential equations. This situation will not in general be encountered but is analogous to the interpretation of Borgman (1967) who in studying forces on structures linearizes nonlinear terms such as $u_i|\vec{u}|$ by $u_i R$ where R is proportional to the

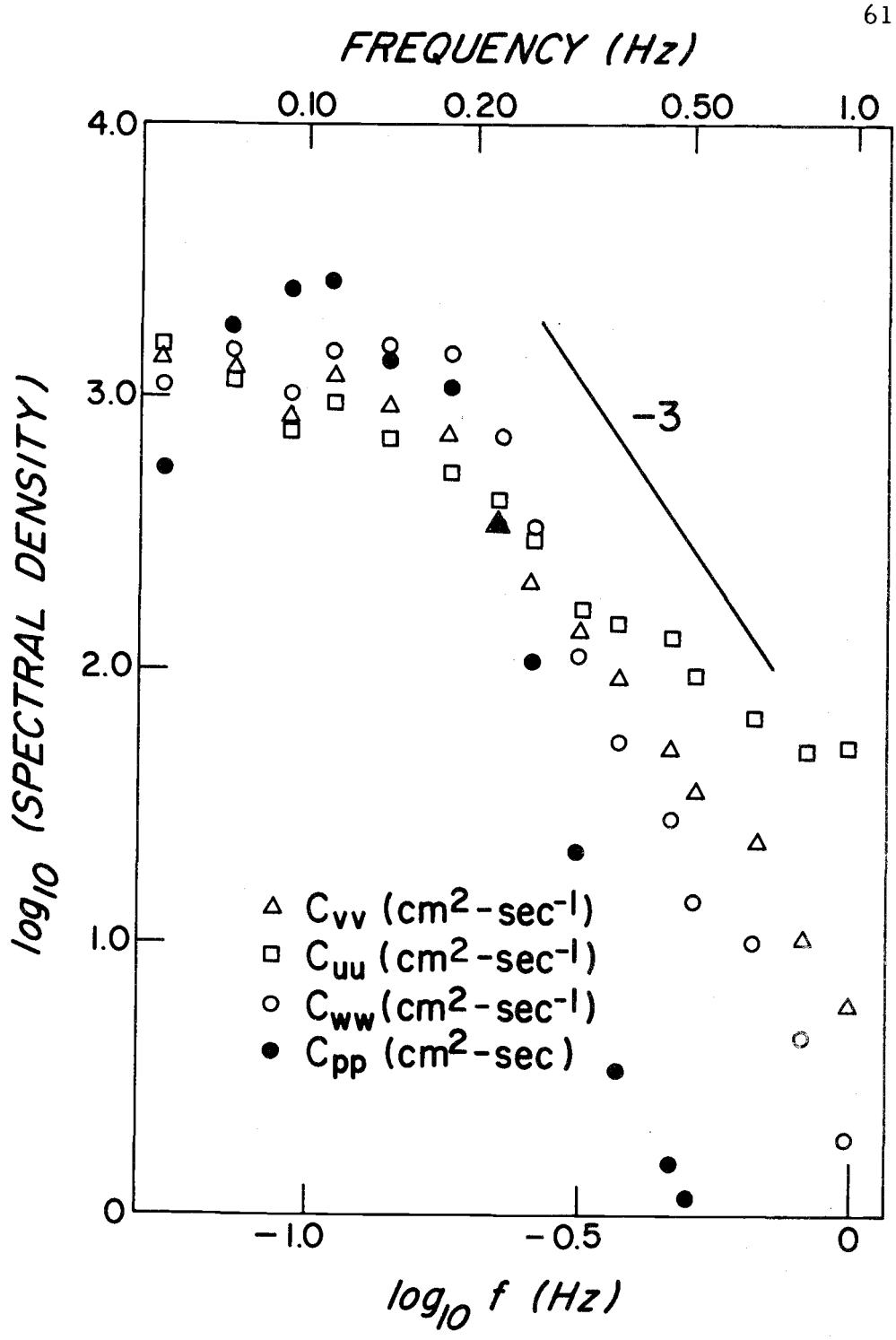

Figure 9. Velocity and pressure spectra.

root mean square wave velocity.

By dimensional analysis, it can be shown that a saturated wave height spectrum should be proportional to σ^{-5} at frequencies above the predominant wave frequency but below the frequencies associated with capillary waves (see, for example, Phillips, 1966, p. 109). In this frequency region, the equilibrium range, the pressure spectrum should be proportional to $\sigma^{-5}e^{2\sigma^2 z/g}$ and the vertical velocity spectrum should be proportional to $\sigma^{-3}e^{2\sigma^2 z/g}$ for deep water gravity waves. An attempt was made to fit these curves to the p and w spectra shown in Figure 9 and no evidence of an equilibrium range was found. Note, however, that the normalized pressure spectrum does fall below the velocity spectra at high frequencies. The v and w spectra do not drop nearly as fast as required for an equilibrium range but drop much faster than one might expect for turbulent spectra. For the frequencies in Figure 9, the turbulence should be in the energy containing region and the velocity spectra should probably be dropping more slowly. Several shallow water wave velocity spectra found by Bowden and White (1966), Simpson (1969), and Shonting (1967, volume 2) also indicate the above intermediate behavior. No one has commented about this intermediate behavior beneath wave but there are several possible explanations. At frequencies above the predominant wave frequency, the velocity spectra away from the surface may not be governed by an equilibrium range (even if one exists for the wave height) but may instead by governed by a nonlinear energy

transfer between the wave components. A spectrum which is proportional to $\sigma^{-3} e^{2\sigma^2 z/g}$ is so steep that real physical nonlinearities would possibly preclude its actual existence. A second explanation may be that the actual velocity spectra are much steeper than those that are observed and the observed spectra may be smeared out due to Doppler shift effects of high frequency wave velocities being superimposed on low frequency wave velocities. In addition, instrumental linearity must be extremely good to detect a spectrum which is proportional to $\sigma^{-3} e^{2\sigma^2 z/g}$. However the fact that several different instruments (with presumably different nonlinearities) give similar results suggest that the result is real rather than an instrumental effect.

Figure 10 shows the normalized pressure energy spectrum, the vertical velocity energy spectrum, and the predicted vertical velocity spectrum that is obtained from the pressure spectrum and Equation 55. The excess of observed velocity energy at and below the predominant wave frequency near 0.1 Hz may be due to TOTEM motion. Also the records are at different times and motions that would show up in both p and w might be different at the two times.

According to Equations 51 through 54, the theoretical phase between w and u and between w and v is $\pm 90°$. From Table 2, most of the energy is between 0.07 Hz and 0.22 Hz and, in this region, the phase between w and v is about 90° but the phase

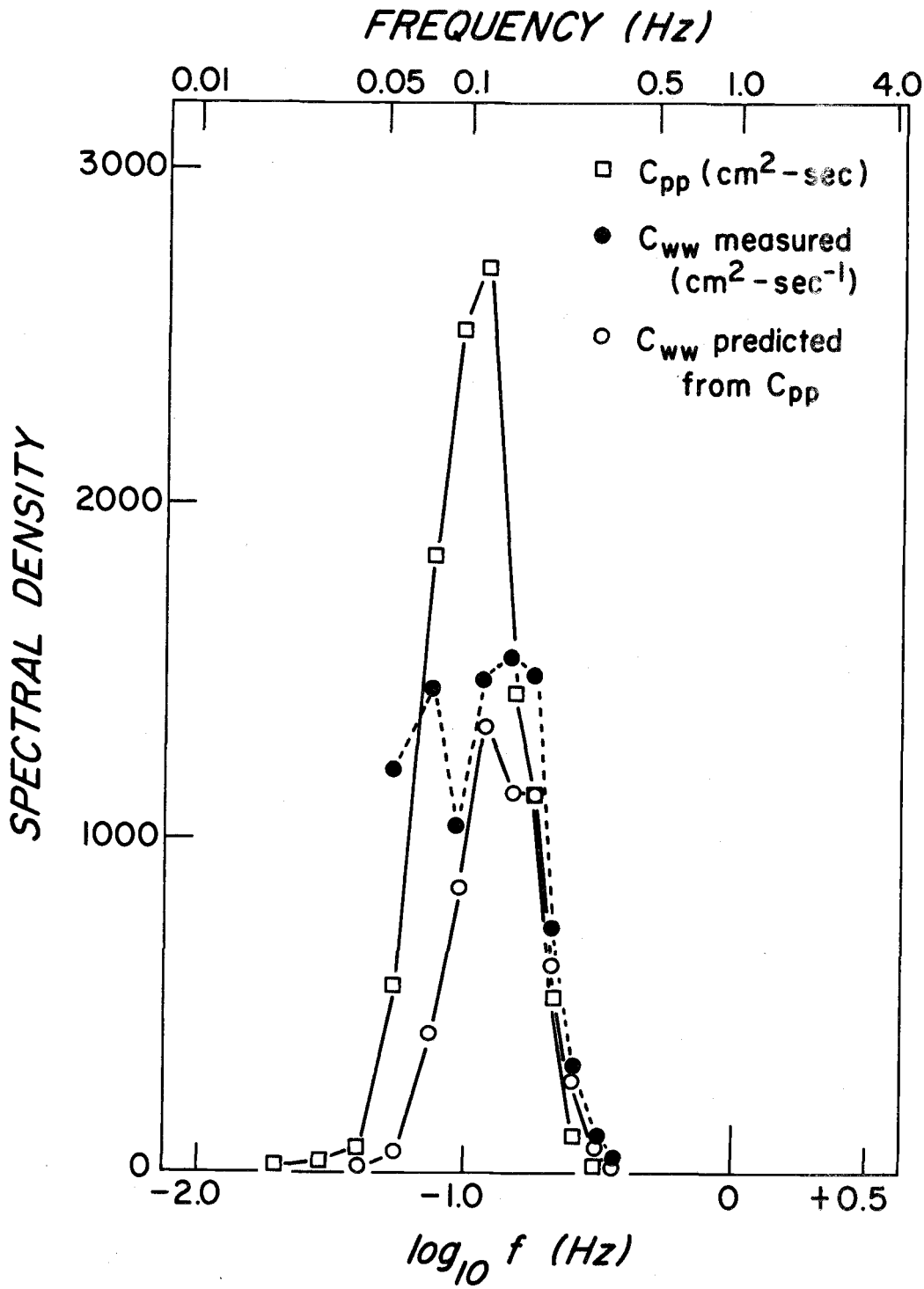

Figure 10. Pressure and vertical velocity spectra.

between w and u shows considerable scatter. The poorer agreement for the phase between w and u may be due to the fact that the dominant wave direction is almost perpendicular to the x direction and, within the frequency bands used for the spectral analysis, there may be phase cancellation from component waves having different component directions along the x axis.

From Equation 54, the following quantity should be unity

$$\left[\frac{C_{ww}(f)}{C_{uu}(f) + C_{vv}(f)}\right]^{1/2} \tag{68}$$

The average value of Expression 68 over the wave frequency band from 0.07 Hz to 0.22 Hz is 0.86 with a standard deviation of 0.16. This result is consistent with the results of Lonquet-Higgins et al. (1963) who find an average value of 0.91 for a quantity similar to Expression 68 but written in terms of the wave height and wave slope spectra instead of the wave velocity spectra. Although the average value is not given, shallow water wave velocity measurements by Simpson (1969) also indicate that Expression 68 is less than unity. For the TOTEM data, the scatter about the average value of Expression 68 may be due to the finite length of the record and to velocities that are not due to waves. Although better agreement with Expression 68 and the theoretical phases between w and u and between w and v could be obtained by slight rotations of the coordinate system,

it was decided not to subjectively alter the final results.

Figure 11 shows the directional spectra at several frequencies as determined from Equation 59. The peaks of the directional spectra are at 75° which is close to the dominant direction of the waves as observed from the ship. The directional spectra are approximately distributed about the prevailing wind direction and become wider on either side of the predominant wave frequency near 0.115 Hz. The solid line in Figure 11 shows the directional spectrum which is obtained from Equation 59 when all of the wave energy is moving in the 75° direction. For this case, the true directional energy spectrum is a delta function at 75° and the directional spectrum shown in Figure 11 illustrates the smoothing effect due to having only five Fourier coefficients. The dotted line in Figure 11 shows the directional spectrum which is obtained when half of the wave energy is moving in the 30° direction and half of the wave energy is moving in the 120° direction. The two theoretical spectra for the special cases have been adjusted in amplitude so that their peaks coincide. Comparing the observed directional spectra to the theoretical directional spectra shows that the waves were relatively shortcrested but seemed to be less so near 0.115 Hz. The shortcrestedness suggests that the waves were mostly local sea and were probably generated during the 10 $m\text{-}sec^{-1}$ to 20 $m\text{-}sec^{-1}$ winds preceding the measurements. Since $\psi(f, \theta)$ is approximately evenly distributed about the y axis, while $\cos \theta$

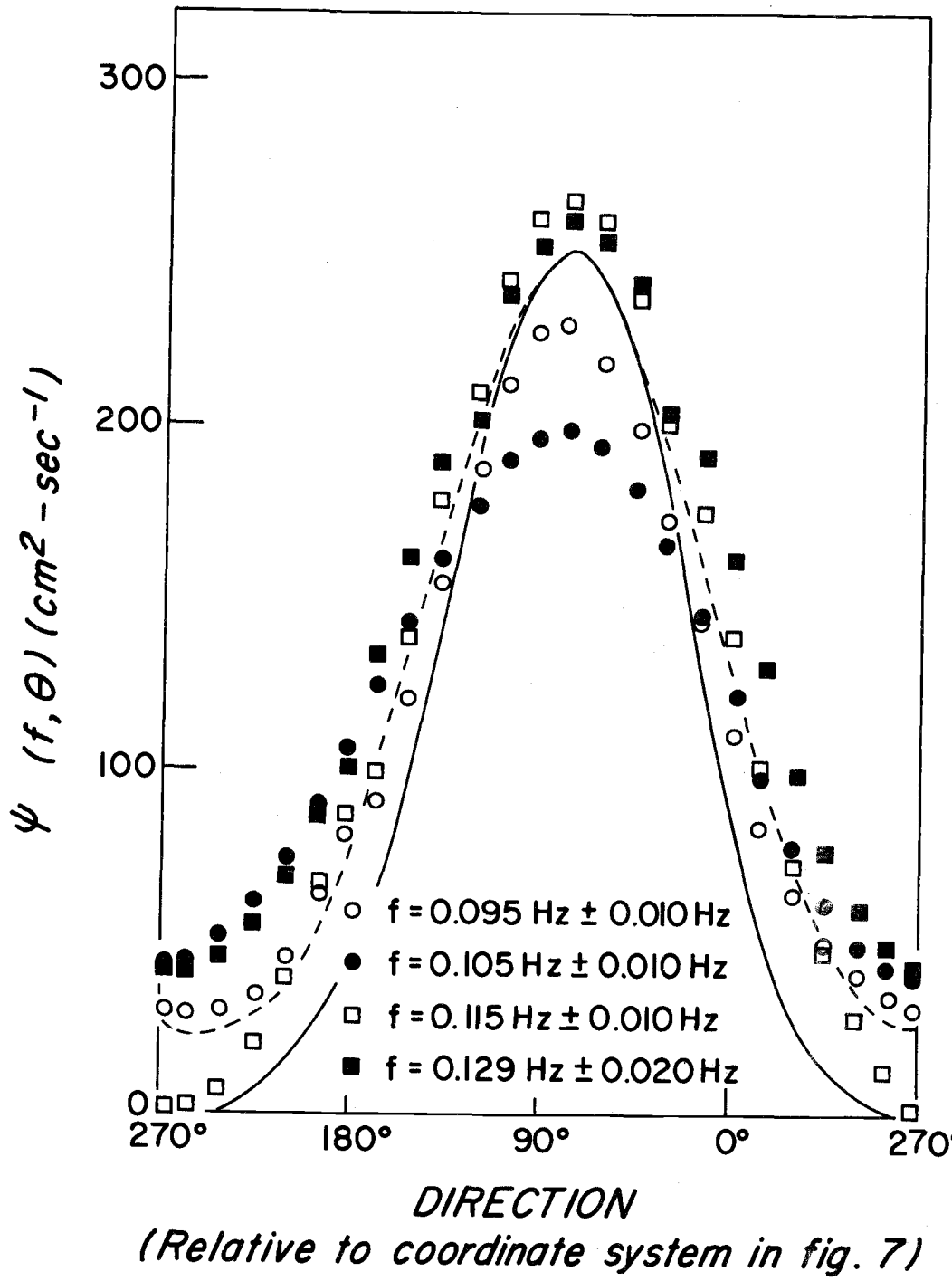

Figure 11. Directional energy spectra.

changes sign, Equation 56 shows that γ^2_{uw} tends to be small and Equation 57 shows that γ^2_{vw} is a measure of the shortcrestedness of the waves. The coherence squared values in Table 2 support this conclusion with γ^2_{vw} having its maximum value near the predominant wave frequency.

VI. TURBULENCE MEASUREMENTS IN A TIDAL CHANNEL

Description of Experiment and Analysis

On March 11, 1970, measurements of turbulent velocity fluctuations were made from a pile in Yaquina Bay, Oregon. Figure 12 shows the experimental arrangement during the measurements. Signals were sent by cable to the Marine Science Center which is several hundred meters from the measurement site. Data was collected and processed in the same way as the TOTEM data. After the experiment, a spring scale was used to check the drag probe's response to static forces and this data is plotted in Figure 3.

Results

Because the drag probe was rigidly attached to a pile, sensor motion was negligible and the errors are those associated with the drag probe. Maximum errors due to the drag probe calibration, hysteresis, and crosstalk are probably about 10%. The mean flow and the turbulence are somewhat affected by the bottom topography and also by other piles near the measurement site. Thus the turbulence observed may not be typical of the whole tidal channel.

A 614 second record (run 1) and a 410 second record (run 2) have been analyzed. Run 1 was made 30 minutes after high tide as

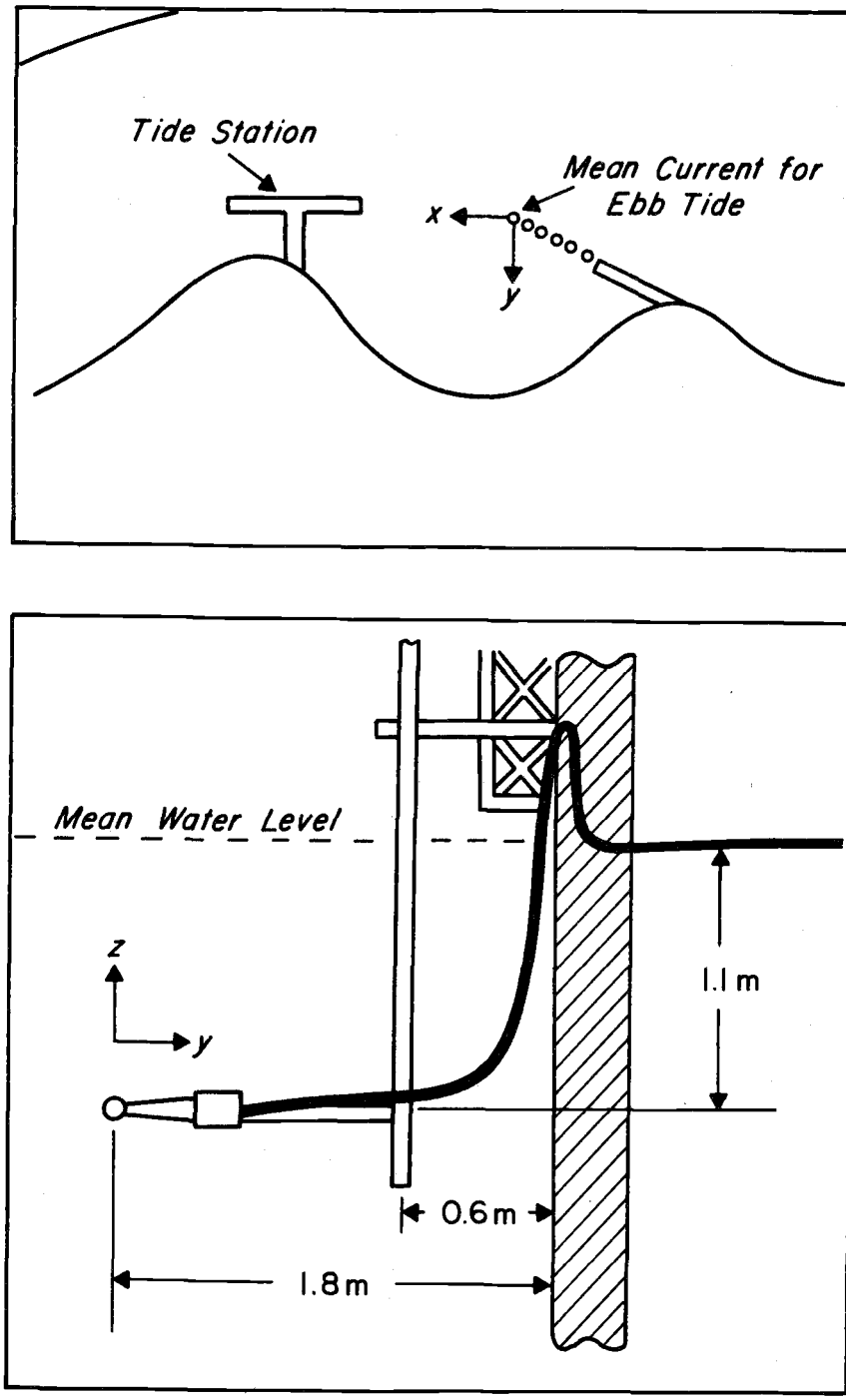

Figure 12. Tidal channel experimental arrangement.

measured at a tide station about 100 m down-stream from the measurement site. Run 2 was made at about the maximum ebb tide. For run 1, the drag probe was approximately 4 m above the bottom and, for run 2, the drag probe was about 3 m above the bottom. For run 1, the mean velocities were: $\overline{w} = 2.4$ cm-sec^{-1}, $\overline{v} = 25.3$ cm-sec^{-1}, $\overline{u} = 57.6$ cm-sec^{-1}. The magnitude of the mean horizontal velocity was 63 cm-sec^{-1}. For run 2, the mean velocities were: $\overline{w} = 5.3$ cm-sec^{-1}, $\overline{v} = 35.0$ cm-sec^{-1}, $\overline{u} = 131$ cm-sec^{-1}. The magnitude of the mean horizontal velocity was 136 cm-sec^{-1}. Taking the distance from the bottom as a length scale, one obtains Reynolds numbers of about 2×10^6 and 3×10^6 for runs 1 and 2 respectively. These Reynolds numbers are believed large enough for an inertial subrange to exist. Because the zero velocity output of the probe could only be obtained by removing it from the water, the mean velocities may be in error by perhaps 25%. For this reason, the mean vertical velocities were ignored and the requirement that the mean vertical velocity $\overline{w}$ be zero if the z axis were vertical was not used to rotate the measurement coordinate system. The direction of the mean horizontal current is thought to be correct to within ±45°. For run 1, the x axis was about -24° from the down-stream direction and, for run 2, the x axis was about -15° from the down-stream direction.

Tables 3 and 4 are a summary of the statistical results.

TABLE 3. Spectral Results for Tidal Channel Data; Run 1

Frequency Hz	Degrees of Freedom	C_{ww} (cm^2-sec^{-1})	C_{uu} (cm^2-sec^{-1})	C_{vv} (cm^2-sec^{-1})	θ_{uw} (°)	γ^2_{uw}	fC_{uw} (cm^2-sec^{-2})	θ_{vw} (°)	γ^2_{vw}	fC_{vw} (cm^2-sec^{-2})	θ_{uv} (°)	γ^2_{uv}	fC_{uv} (cm^2-sec^{-2})
.0098	12	7539	6941	7611	148	.092	-18.2	169	.733	-62.1	36	.273	29.9
.0195	12	1992	8295	2719	169	.221	-36.6	159	.537	- 3.11	24	.131	30.5
.0293	12	1018	2670	594	239	.045	- 5.29	207	.508	-14.5	323	.010	9.34
.0391	12	998	3679	830	185	.379	-46.0	178	.621	- 2.80	331	.102	19.1
.0537	24	659	2384	222	53	.156	+15.8	180	.753	-17.9	127	.166	-9.53
.0732	24	628	1305	315	250	.212	-10.7	198	.522	-22.4	326	.249	19.4
.0928	24	294	634	139	312	.076	+ 7.32	182	.649	-15.1	172	.079	-7.69
.1123	24	222	569	67.7	206	.024	- 5.56	180	.668	-11.3	334	.098	6.21
.1416	48	257	537	117	165	.052	-11.6	176	.707	-20.5	15	.115	11.6
.1807	48	132	251	91.2	177	.150	-12.8	181	.515	-14.2	356	.199	12.2
.2197	48	74.8	121	50.2	186	.042	- 4.28	169	.615	-10.4	356	.032	3.05
.2588	48	58.2	145	35.9	187	.050	- 5.28	162	.560	- 8.42	317	.046	2.91
.3174	96	58.1	63.2	36.4	207	.109	- 5.68	164	.791	-12.5	317	.102	3.55
.3955	96	34.3	38.0	18.4	202	.114	- 4.45	165	.735	- 8.23	315	.127	2.64
.4736	96	18.6	23.6	12.1	198	.116	- 3.21	159	.738	- 5.68	333	.151	2.78
.5518	96	19.0	14.2	10.7	182	.066	- 2.33	159	.713	- 6.24	317	.093	1.52
.6690	192	13.3	8.97	7.31	203	.058	- 1.62	162	.694	- 5.23	314	.113	1.27
.8252	192	5.40	3.42	3.81	200	.059	- .807	157	.656	- 2.72	315	.141	.787
.9815	192	2.65	2.21	2.23	197	.113	- .764	159	.658	- 1.80	319	.140	.616
1.1377	192	2.06	1.12	2.03	215	.166	- .578	154	.747	- 1.80	295	.176	.304
1.3721	384	.920	.612	0.915	191	.098	- .317	155	.645	- .917	319	.090	.233
1.6846	384	.468	.297	.444	192	.043	- .128	164	.656	- .632	311	.057	.102
1.9971	384	.299	.188	.277	199	.046	- .096	166	.625	- .441	314	.057	.076
2.3096	384	.212	.136	.201	212	.042	- .068	169	.591	- .360	285	.060	.024
2.7783	768	.143	.082	.126	194	.028	- .048	174	.600	- .286	326	.018	.031
3.4033	768	.101	.057	.083	193	.033	- .056	176	.594	- .235	329	.022	.029
4.0283	768	.080	.044	.059	183	.039	- .074	179	.587	- .211	347	.029	.033
4.6533	768	.073	.038	.053	180	.044	- .052	180	.606	- .226	359	.027	.034

TABLE 4. Spectral Results for Tidal Channel Data, Run 2

Frequency Hz	Degrees of Freedom	C_{ww} (cm^2-sec^{-1})	C_{uu} (cm^2-sec^{-1})	C_{vv} (cm^2-sec^{-1})	θ_{uw} (°)	γ^2_{uw}	fC_{uw} (cm^2-sec^{-2})	θ_{vw} (°)	γ^2_{vw}	fC_{vw} (cm^2-sec^{-2})	θ_{uv} (°)	γ^2_{uv}	fC_{uv} (cm^2-sec^{-2})
.0098	8	793	216	3074	275	.026	+ .101	178	.967	-15.0	176	.002	- .317
.0195	8	69.1	364	232	143	.420	-1.60	192	.895	- 2.28	63	.531	1.90
.0293	8	668	164	2244	19	.852	+ .860	182	.977	-35.4	19	.843	15.5
.0391	8	219	301	835	182	.276	-5.27	188	.909	-15.8	27	.119	6.03
.0537	16	104	85.0	528	229	.034	- .611	184	.925	-12.0	312	.005	.561
.0732	16	60.0	69.8	264	205	.081	-1.22	192	.907	- 8.60	340	.052	2.13
.0928	16	18.9	62.5	107	158	.299	-1.62	196	.836	- 3.79	20	.213	3.28
.1123	16	28.8	90.2	156	195	.135	-2.03	197	.876	- 6.75	354	.026	2.14
.1416	32	21.2	48.9	110	176	.308	-2.45	193	.798	- 5.95	36	.279	4.44
.1807	32	13.2	22.0	81.5	137	.035	- .421	181	.793	- 5.27	67	.034	.559
.2197	32	5.63	12.5	30.2	156	.097	- .527	164	.530	- 2.03	358	.109	1.41
.2588	32	6.75	14.1	49.3	149	.252	-1.08	179	.753	- 4.10	20	.307	3.55
.3174	64	2.88	7.94	19.4	139	.030	- .197	192	.684	- 1.92	71	.096	.401
.3955	64	2.79	5.21	10.4	189	.206	- .676	195	.812	- 1.86	4	.087	.859
.4736	64	1.59	2.06	8.72	173	.142	- .320	202	.771	- 1.43	50	.200	.572
.5518	64	1.16	2.59	7.70	181	.185	- .416	195	.753	- 1.38	24	.233	1.09
.6690	128	.791	2.40	6.42	155	.164	- .308	192	.731	- 1.26	35	.210	.988
.8252	128	.249	.953	1.81	146	.027	- .060	192	.686	- .449	21	.040	.203
.9815	128	.215	.954	1.82	168	.008	- .038	194	.658	- .483	18	.148	.474
1.1377	128	.140	1.01	1.33	130	.119	- .094	189	.558	- .362	25	.292	.649
1.3721	256	.071	.751	.758	114	.170	- .053	189	.572	- .239	33	.266	.447
1.6846	256	.035	.832	.424	109	.138	- .035	185	.471	- .140	22	.368	.562
1.9971	256	.019	.891	.297	92	.163	- .004	168	.308	- .081	17	.521	.709
2.3096	256	.013	.710	.185	63	.076	+ .027	169	.174	- .046	17	.563	.599
2.7783	512	.009	.446	.104	40	.062	+ .034	181	.236	- .004	11	.409	.376
3.4033	512	.006	.279	.061	20	.061	+ .033	177	.209	- .030	8	.467	.299
4.0283	512	.005	.212	.043	13	.048	+ .027	177	.264	- .030	5	.463	.260
4.6533	512	.004	.192	.037	5	.053	+ .031	179	.256	- .030	2	.478	.271

Because there are only six files in run 1 and four files in run 2, there is not enough information to accurately study the variation of the final spectral estimates and thus the theoretical degrees of freedom are given in the tables. The velocity spectra are plotted in Figures 13 and 14 and appear to have regions where they are approximately proportional to $f^{-5/3}$. The reference line in Figures 13 and 14 has a slope of $-5/3$. For run 1, the scale sizes were less than 22 cm, the scale size at which the probe response is theoretically 3 db down, for frequencies greater than approximately 3 Hz and, hence, the roll-offs at higher frequencies in Figure 13 are probably instrumental. For run 2, the scale sizes were greater than 22 cm for frequencies below about 6 Hz and the roll-off of the vertical velocity in Figure 14 may be partly real. For run 2, a resistance wire wave staff was used to measure the surface wave height and the small bumps in the spectra at 0.26 Hz are probably due to wave motion. The least square slopes and their 90% confidence levels as estimated from the t distribution of the velocity spectra for frequencies between 0.05 Hz and 1.0 Hz are given below. The lower limit was chosen to exclude the lower four frequency bands where there are not many degrees of freedom and the scales are strongly affected by the surface and the bottom and the upper limit was chosen to exclude regions where the spectra are affected by instrument response. Because of the type of band averaging used to compute the spectra, the spectral estimates at

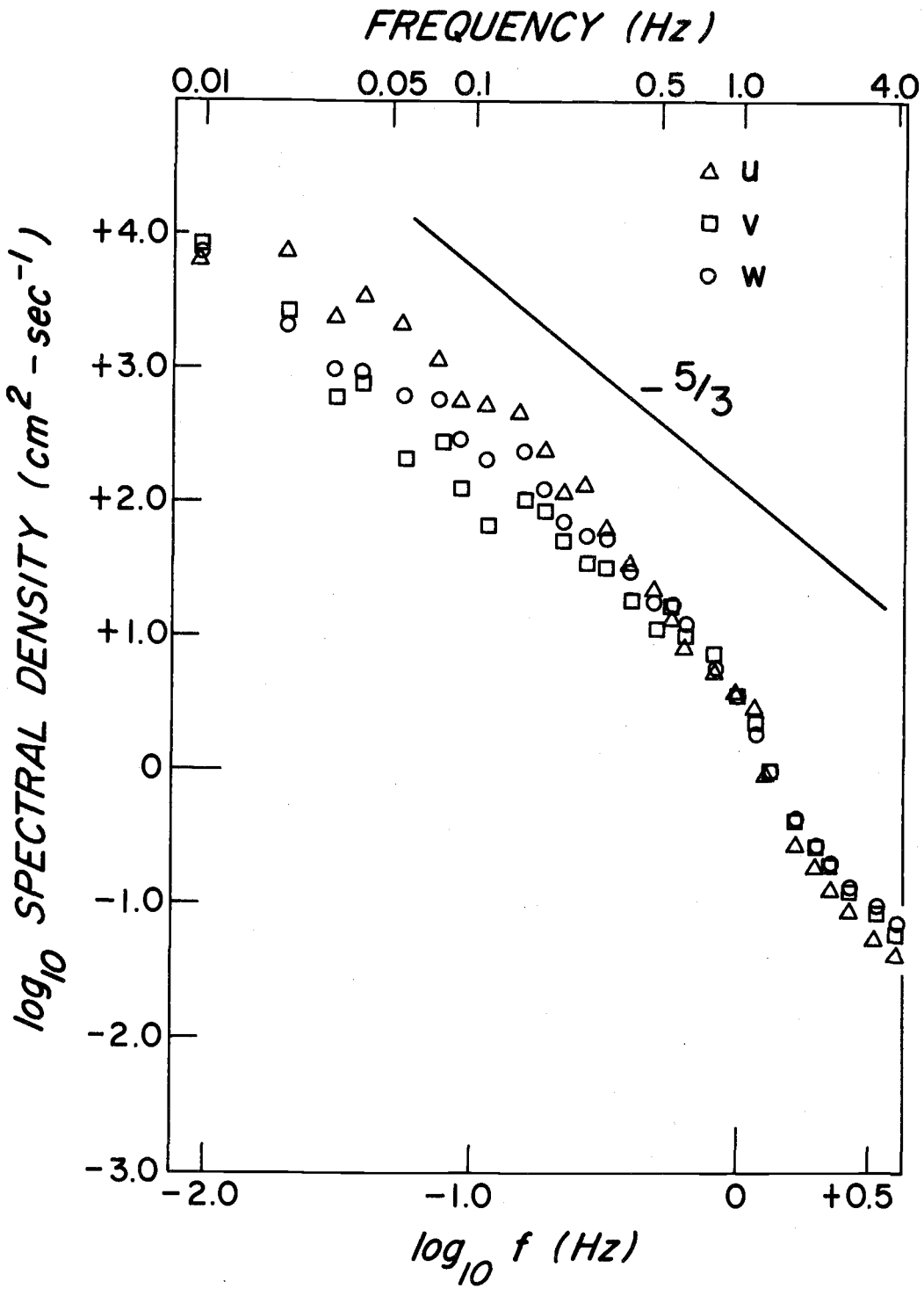

Figure 13. Velocity spectra, run 1.

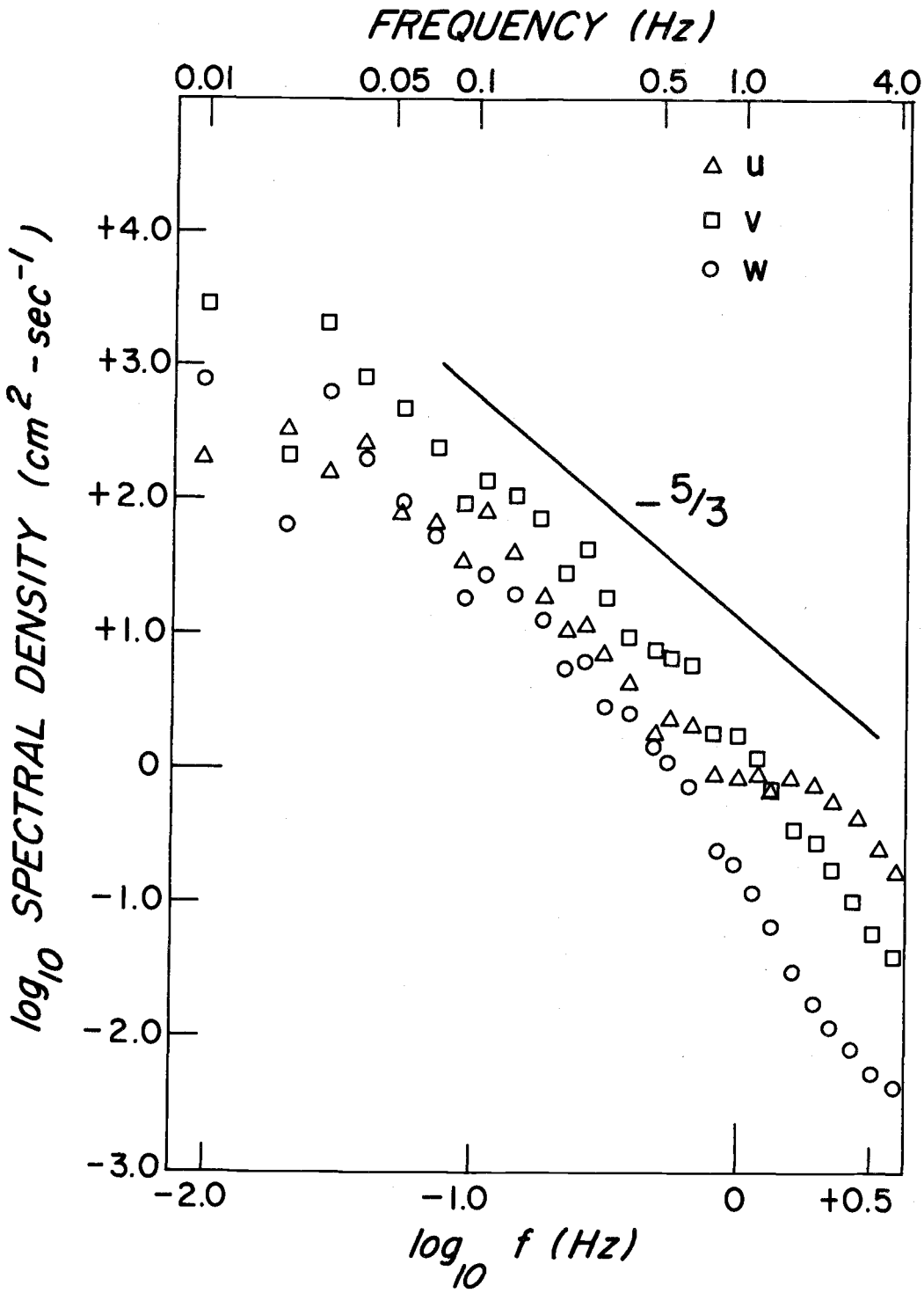

Figure 14. Velocity spectra, run 2.

higher frequencies contain more information than the spectral estimates at lower frequencies. The variance about the least squares line was thus examined as a function of frequency to determine if the higher frequency spectral estimates should be weighted more than the lower frequency spectral estimates. Since the variance did not show a tendency to decrease with increasing frequency, no weighting was used.

	Spectrum	Slope	90% Confidence Lower	90% Confidence Upper
Run 1	u	-2.36	-2.19	-2.53
	v	-1.59	-1.40	-1.78
	w	-1.81	-1.65	-1.97
Run 2	u	-1.76	-1.56	-1.96
	v	-1.90	-1.72	-2.08
	w	-2.01	-1.77	-2.25

For both runs 1 and 2 Taylor's hypothesis yields length scales throughout the frequency spectrum which are not small compared to the distance from the bottom and from the surface. It is thus likely that the turbulent flow was anisotropic and that the actual vertical velocity fluctuations were much smaller than the actual fluctuations in the x and y directions. From Tables 3 and 4, the coherence squared values γ^2_{wv} between w and v seem large for turbulence. For run 1, a second drag probe was in operation 41 cm above the drag probe that is shown in Figure 12. This additional drag probe measured fluctuations showing a similar high coherence squared between

w and v. A possible explanation for the observed vertical velocity fluctuations not being smaller than the horizontal velocity fluctuations and the large γ^2_{wv} values is that the drag probe was tilted with respect to the plane of the large magnitude fluctuations. If the turbulence was distorted by the bottom, this plane need not have been horizontal. To see the effects of tilts, consider the spectral estimates for two velocity components u'_1 and u'_2 which have been obtained by rotating the velocity components u_1 and u_2 an angle Δ in the 1, 2 plane

$$C'_{11} = C_{11}\cos^2\Delta + C_{22}\sin^2\Delta - C_{12}\sin 2\Delta \tag{69}$$

$$C'_{22} = C_{11}\sin^2\Delta + C_{22}\cos^2\Delta + C_{12}\sin 2\Delta \tag{70}$$

$$C'_{12} = \frac{1}{2}(C_{11}-C_{22})\sin 2\Delta + C_{12}\cos 2\Delta \tag{71}$$

$$Q'_{12} = Q_{12} \tag{72}$$

in which C_{ij} is the cospectrum between the unrotated velocity components u_i and u_j, Q_{ij} is the quadrature spectrum between the unrotated velocity components, C'_{ij} is the cospectrum between the rotated velocity components u'_i and u'_j, and Q'_{ij} is the quadrature spectrum between the rotated velocity components. For $\Delta = 0°$, let C_{12} and Q_{12} be zero and $C_{11} = 10\, C_{22}$. The coherence squared between the velocity components in the unrotated frame is

zero. For $\Delta = 45°$, Q'_{12} is zero, $C'_{12} = 4.5\ C_{22}$, $C'_{11} = 5.5\ C_{22}$, and $C'_{22} = 5.5\ C_{22}$. In the rotated frame, the coherence squared between the velocity components is 0.67. As C_{22} becomes negligible in comparison to C_{11} the coherence squared in the rotated frame ($\Delta = 45°$) approaches unity.

Although the complicated flow situation relative to the drag probe makes it difficult to interpret the directions of momentum fluxes, some approximate estimates may be made. From Tables 3 and 4, the cospectra between u and w and between v and w are almost always negative. Thus, there is a downward flux of x directed momentum and of y directed momentum. The cospectra between u and v are positive and may thus indicate a flux of x directed momentum in the positive y direction. These momentum fluxes would occur if the outgoing tide and river flow were such that the horizontal velocity decreased toward the bottom and the x component of horizontal velocity decreased in the positive y direction toward the shore.

The velocity spectra in Figures 13 and 14 show a f^{-1} to f^{-2} behavior which is typical of turbulence and, except for the small bumps at 0.26 Hz in Figure 14, there is no indication of wave motion. If the velocity fluctuations were all due to turbulence, Equation 26 would probably be better than Equation 28 for computing the velocity components from the measured force components. Equation 26 uses

the approximation that the total derivative is negligible whereas Equation 28 approximates the total acceleration by the local acceleration. Since in a turbulent flow with a large mean velocity the local derivative is much larger than the total derivative, Equation 26 is a better approximation. However, because of the large mean flow, the drag forces dominate and both equations should give similar results.

To determine whether Equation 26 yielded solutions significantly different than those obtained from Equation 28, Equation 26 was also used to obtain velocities for short sections of the tidal channel data. For the down-stream velocity component, the solutions were nearly identical. For the cross-stream and vertical components, the solutions were essentially identical below 1 Hz but, above 1 Hz, the spectra of the velocities obtained from Equation 28 showed a somewhat greater decrease with increasing frequency than the spectra of the velocities obtained from Equation 26. The numerical integration used to solve Equation 28 filters out the higher frequencies of the measured forces. For the down-stream component, the large mean velocity prevented velocity zero crossings and, hence, the inertial force term was not important and the solutions to Equations 26 and 28 were almost identical. For the cross-stream and vertical components zero crossings occur and the high frequencies are somewhat affected. For the tidal channel data, the solutions to Equations 26 and 28 were virtually identical below 1 Hz so that either equation gave acceptable results in the region unaffected by instrument response effects.

VII. DISCUSSION AND CONCLUSION

Experimental Results

The experimental results indicate that the drag probe used was a suitable instrument for the measurement of velocity fluctuations caused by ocean gravity waves and by turbulence. For the wave measurements, there were experimental errors due to the motion of the buoy, wave reflection, and possible nonalignment of one drag probe axis with the vertical. These errors were not due to the instrument and are difficult to overcome when making measurements in the open ocean. Within the errors of the experiment, it was found that linear wave theory was adequate to describe the relations between the wave pressure and the wave velocity components. This result is expected because of the small amplitudes of the waves. The root mean square wave pressure at a depth of 5.5 m was 17.2 cm of water. The velocity spectra decrease with increasing frequency was roughly proportional to f^{-3} and was not as rapid as the decrease expected for equilibrium range type limitations. Above the predominant wave frequency, possible explanations are: 1. The velocity field may be affected by nonlinearities. 2. The observed spectra may be smeared out by Doppler shift effects due to high frequency wave velocities being superimposed on lower frequency wave velocities. 3. Instrumental nonlinearities may prevent the velocity spectra from falling as

steeply as expected for an equilibrium range. Measurements of the wave velocity components were used to obtain estimates of the directional energy spectrum and the shortcrestedness of the sea. Because only the first five Fourier coefficients of the directional energy spectrum can be obtained from measurements of the velocity components, the directional spectrum was highly smoothed.

For the turbulence measurements in a tidal channel, it is difficult to determine a proper reference coordinate system because of the complicated horizontal and vertical velocity shears and the unknown influence of piles and bottom topography on the flow. The velocity spectra decrease with increasing frequency was generally somewhat greater than $f^{-5/3}$. Because of the complicated flow situation and the influence of boundaries, there is no theoretical reason why the spectra should be exactly proportional to $f^{-5/3}$. The results are consistent with numerous other observations that turbulent spectra usually show a f^{-1} to f^{-2} behavior in the energy containing region.

Suggested Drag Probe Modifications

Although the experimental results demonstrate the usefulness of the drag probe approach, there are several desirable modifications for the instrument that was used, especially for measurements of turbulence in the ocean. As an example, the magnitude of the water velocity fluctuations necessary to support a flux of 1 dyne-cm^{-2} (a

typical wind stress) through the upper ocean is of order 1 cm-sec^{-1}. Because of the presence of much larger wave velocities, the instrument must have a large dynamic range with high linearity and a low noise level.

A major problem of the drag probe is its hysteresis and lack of suitability for measurements of slowly varying and mean velocities. This problem is mainly due to the compressed sponge rubber supports. A second problem with the sponge rubber used is that it deteriorates after prolonged exposure to salt water and must eventually be replaced. Springs of stainless steel wire could possibly be used in place of the sponge rubber. Six springs could be symmetrically placed between the spheres and the probe support could pass through the center of one of the springs. Sections of a nondeteriorating type of rubber could be placed between the spheres to provide any desired damping. If the drag probe can be used to accurately measure mean velocities, the mean velocities may be used as criteria for correcting errors in the final measurement results which are due to not aligning the axes of the drag probe with the desired coordinate system. As an example, for wave and turbulence measurements, one can rotate the measurement coordinate system during analysis so that the time averaged vertical velocity is zero as is theoretically expected. Since it is difficult for divers to accurately level the drag probe, the accurate measurements of any mean velocities is necessary for

interpreting and possibly correcting the final results. The crosstalk of the instrument can be reduced by more careful manufacture of the sensor head so that the plane of each ferrite disk is more nearly perpendicular to the axis of its corresponding inductor.

For measurements of wave and turbulent velocities it may not always be possible to align the drag probe so that wake effects due to the electronics case are negligible. A different configuration could greatly reduce wake effects. Because the circuit is simple and has few components, the electronics could be fitted easily into a long thin probe support only a few cm in diameter. Another solution is to mount the probe head on a long thin rigid rod and to have the electronics case some distance away. The latter solution requires care because one is measuring the amplitude modulation of a high frequency signal and long cables may increase noise pickup and crosstalk between channels. It is also desirable to keep the entire instrument as compact as possible so that divers may easily handle it.

Since it is thought that some eddy shedding may take place with the present reasonably smooth outer sphere, calibrations should be carried out with roughened spheres and perforated spheres. In studying the influence of the type of sphere on the performance of a thrust anemometer for use in the atmosphere, Doe (1963) found that a perforated sphere greatly reduced eddy shedding flutter.

BIBLIOGRAPHY

Adelfang, S. I. 1969. Measurements of atmospheric turbulence a few meters above the sea surface with a three component thrust anemometer. New York University, School of Engineering and Science Report TR-69-3. 73 p.

Beardsley, G.F. Jr., G. C. Knollmen, A.S. Homanoto, and J. D. Eisler. 1963. Device for measuring particle velocities in an underwater wave field. Review of Scientific Instruments 34:516-519.

Blackman, R. B. and J. W. Tukey. 1958. The measurement of power spectra. New York, Dover Publications. 190 p.

Borgman, L. E. 1967. Spectral analysis of ocean wave forces on piling. Journal of the Waterways and Harbors Division ASCE 93:129-156.

Bowden, K. F. 1962. Measurements of turbulence near the sea bed in a tidal current. Journal of Geophysical Research 67:3181-3186.

Bowden, K. F. and L. A. Fairbairn. 1956. Measurements of turbulent fluctuations and Reynolds stresses in a tidal channel. Proceedings of the Royal Society of London A237:422-438.

Bowden, K. F. and R. A. White. 1966. Measurements of the orbital velocities of sea waves and their use in determining the directional spectrum. Geophysical Journal of the Royal Astronomical Society 12:33-54.

Doe, L. A. E. 1963. A three-component thrust anemometer for studies of vertical transports above the sea surface. Bedford Institute of Oceanography Report 63-1. 87 p.

Eagleson, P.S. and W. P. M. Van de Watering. 1964. A thermistor probe for measuring particle orbital speed in water waves. United States Army Coastal Engineering Research Center Technical Memorandum 3. 50 p.

Earle, M. D., J. Groelle and G. F. Beardsley, Jr. 1970. A three component drag probe for the measurement of turbulent water velocity fluctuations. Review of Scientific Instruments 41:1021-1025.

Grace, R. A. and F. M. Casciano. 1969. Ocean wave forces on a subsurface sphere. Journal of the Waterways and Harbor Division, ASCE. 95:291-317.

Grant, H. L., R. W. Stewart and A. Moilliet. 1962. Turbulence spectra from a tidal channel. Journal of Fluid Mechanics 12:241-268.

Hamming, R. W. 1965. Numerical methods for scientists and engineers. New York, McGraw-Hill. 411 p.

Hinze, J. O. 1959. Turbulence. New York, McGraw-Hill. 586 p.

Inman, D. L. and N. Nasu. 1956. Orbital velocity associated with wave action near the breaker zone. Department of the Army, Corps of Engineers, Beach Erosion Board. Technical Memorandum 79, 43 p.

Keulegan, G. H. and L. H. Carpenter. 1958. Forces on cylinders and plates in an oscillating fluid. Journal of Research National Bureau of Standards 60:423-440.

Kirwan, A. D. Jr., S. Adelfang, and G. J. McNally. 1966. Laboratory and field evaluation of a thrust anemometer. New York University, Geophysical Science Report 66-10.

Lamb, H. 1935. Hydrodynamics. New York, Dover Publications. 738 p.

Lonquet-Higgins, M. S. 1962. The directional spectrum of ocean waves and processes of wave generation. Proceedings of the Royal Society of London A265:286-315.

Lonquet-Higgins, M. S., D. E. Cartwright and N. D. Smith. 1963. Observations of the directional spectrum of sea waves using the motions of a floating buoy. In: Ocean Wave Spectra, Prentice-Hall Inc., Englewood Cliffs, N. J. 111-132.

Lukasik, S. J. and C. E. Grosch. 1963. Pressure-velocity correlations in ocean swell. Journal of Geophysical Research 68:5689-5699.

McNally, G. R. 1970. A thrust anemometer for the measurement of the turbulent wind vector. New York University, School of Engineering and Science. Report TR-70-1. 43 p.

Michell, J. H. 1893. The highest waves in water. Philosophical Magazine 36:430-437.

Miller, R. L. and J. M. Zeigler. 1964. The internal velocity field in breaking waves. Proceedings of the 9th Conference on Coastal Engineering. ASCE. p. 103-122.

Morse, P. M. 1936. Vibration and sound. New York, McGraw-Hill.

Nagata, Y. 1964. The statistical properties of orbital wave motions and their application for the measurement of directional wave spectra. Journal of the Oceanographical Society of Japan 19:169-181.

Nagata, Y. 1964. Observations of the directional wave properties. Coastal Engineering in Japan 7:11-30.

Nath, J. H. and S. Neshyba. 1970. Two point mooring system for a spar buoy. Preprint of paper given at ASCE National Structural Engineering Meeting, Portland, Oregon. 13 p.

Neshyba, S., D. A. Young and J. H. Nath. 1970. Moored spar buoys for ocean research. Oceanology 2:22-26.

O'Brien, M. P. and J. R. Morison. 1952. The forces exerted by waves on objects. Transactions of the American Geophysical Union 33:32-38.

Patterson, A. M. 1958. Turbulence spectrum studies in the sea with hot wires. Journal of Limnology and Oceanography 3:171-180.

Phillips, O. M. 1966. The dynamics of the upper ocean. Cambridge, G. B., Cambridge University Press. 261 p.

Shonting, D. H. 1967. Observations of particle motions in ocean waves. Naval Underwater Weapons Research and Engineering Station Technical Memorandum 377. 2 Vol., 176 p.

Simpson, J. H. 1969. Observations of the directional characteristics of sea waves. Geophysical Journal of the Royal Astronomical Society 17:93-120.

Smith, S. D. 1966. Thrust anemometer measurements of wind velocity fluctuations, spectra and stress over the sea. Bedford Institute of Oceanography Report 66-8, 153 p.

Smith, S. D. 1967. Thrust anemometer measurements of wind velocity, spectra and of Reynolds stress over a coastal inlet. Journal of Marine Research 25:239-262.

Stewart, R. W. and H. L. Grant. 1962. Determination of the rate of dissipation of turbulent energy near the sea surface in the presence of waves. Journal of Geophysical Research 67:3177-3180.

Suzuki, Y. 1968. Determination of approximate directional spectra for surface waves. University of California, Berkeley, Hydraulic Engineering Laboratory Report 1-111. 47 p.

Thomson, W. T. 1965. Vibration theory and applications. Englewood Cliffs, N. J. Prentice Hall. 384 p.

Wiegel, R. L. 1964. Oceanographical engineering. Englewood Cliffs, N. J. Prentice Hall. 532 p.